SEMMELWEIS EGYETEM DOKTORI ISKOLA

Ph.D. értekezések

3332.

BŐSZ EMÍLIA

Neuromorfológia és sejtbiológia

című program

Programvezető: Dr. Alpár Alán, egyetemi tanár

Témavezető: Dr. Acsády László, csoportvezető

A CORTICO-SUBCORTICAL LOOP FOR MOTOR CONTROL VIA THE PONTINE RETICULAR FORMATION

PhD thesis

Emília Bősz

János Szentágothai Neurosciences Division Semmelweis University





Supervisor: László Acsády D.Sc

Official reviewers: Alán Alpár MD, D.Sc

Magor László Lőrincz D.Sc

Head of the Complex Examination Committee:

Dániel Bereczki MD, D.Sc

Members of the Complex Examination Committee:

Emília Madarász D.Sc Árpád Dobolyi D.Sc

Budapest 2025

TABLE OF CONTENTS

LIST (OF ABBREVIATIONS	. 6
1. IN	VTRODUCTION	. 8
1.1.	General introduction	. 8
1.2.	Theoretical background	10
1.2.1.	Basal ganglia loops	10
1.2.2.	Reticular formation	11
1.2.3.	Intralaminar and parafascicular thalamus	14
1.2.4.	Inhibitory connections between PRF and IL/Pf	17
2. O	BJECTIVES	19
3. M	ETHODS	20
3.1.	Animal housing	20
3.2.	Surgeries	20
3.2.1.	Anesthesia	20
3.2.2.	Virus injections and fiber-optic implantations	20
3.3.	. Histology	22
3.3.1.	Perfusion and tissue fixation	22
3.3.2.	Immunohistochemistry	23
3.4.	Microscopy	24
3.4.1.	Fluorescent microscopy	24
3.4.2.	Confocal microscopy	24
3.4.3.	Electron microscopy	25
3.5.	. In vivo electrophysiology	25
3.5.1.	Cortical activation and LFP recording	25
3.5.2.	Juxtacellular recording	26

	3.6.	Janelia Mouse Light Neuron Browser	26
	3.7.	Behavior	27
	3.8.	Analysis	27
3.	8.1.	Density mapping analysis	27
3.	8.2.	Terminal analysis	28
3.	8.3.	Axonal density analysis	28
3.	8.4.	Analysis of juxtacellular recording	28
3.	8.5.	Video analysis for behavior	29
3.	8.6.	Statistics	30
	3.9.	Funding	30
4.	RI	ESULTS	31
	4.1.	M2/cingulate cortical neurons innervate PRF/GlyT2+ neurons	31
	4.2.	Ultrastructural and quantitative comparison of synaptic terminals in the PRF	36
	4.3.	Thalamus-projecting PRF cells	40
	4.4.	Co-innervation of PRF and the thalamic targets of PRF by L5 neurons	42
	4.5.	Activation of PRF/GlyT2+ neurons promotes rotational movements	49
	4.6.	Distinct projection patterns of thalamus projecting PRF/GlyT2+ cells	58
	4.7.	Electrophysiological recordings of M2 neurons	63
5.	DI	ISCUSSION	67
	5.1.	Overview	67
	5.2.	BG-thalamus and PRF-thalamus circuits in motor regulation	69
	5.3.	Limitations of the study	71
6.	CO	ONCLUSION	73
7.	SU	JMMARY	74
Q	ΡI	FEERENCES	75

9.	BIBLIOGRAPHY OF PUBLICATIONS	84
10.	ACKNOWLEDGEMENTS	85

LIST OF ABBREVIATIONS

ABC Avidin biotinylated horseradish peroxidase complex

AP Anteroposterior

APs Action potentials

ARAS Ascending reticular activating system

BAC Bacterial artificial chromosome

BG Basal ganglia

BSA Bovine serum albumin

C-BG-T Cortico - basal ganglia - thalamocortical

C-PRF-T Cortico - pontine reticular formation – thalamus

CnF Cuneiform nucleus

Cg Cingulate cortex

ChR2 Channelrhodopsin-2

DBS Deep brain stimulation

DAB 3,3'-diaminobenzidine

DiI 1,1'-Dioctadecyl-3,3,3',3'-Tetramethylindocarbocyanine Perchlorate

DIO Double-floxed inverted open reading frame

DV Dorsoventral

eGFP Enhanced Green Fluorescent Protein

EM Electron microscopy

eNpHR Enhanced Natronomonas pharaonis halorhodopsin

EYFP Enhanced yellow fluorescent protein

fDIO FLEX switch double-floxed inverted open reading frame

FIJI Fiji is Just ImageJ

FlpO Flippase recombinase

fps Frames per second

GABA Gamma-aminobutyric acid

Gi Gigantocellular nucleus

GlyR Glycine receptor

GlyT2 Glycine transporter 2

hGH Human growth hormone

HGHpA Human growth hormone polyadenylation signal

hSyn Human synapsin promoter

IL/Pf Intralaminar and parafascicular complex of the thalamus

imTha Intralaminar and medial nuclei IPSC Inhibitory postsynaptic currents

IQR Interquartile range

L5 Layer 5 (of the cortex)

LFP Local field potential

LPGi Lateral paragigantocellular nucleus

M2 Secondary motor cortex

MFR Mean firing rate

ML Mediolateral

MLR Mesencephalic locomotor region

MOs5 Secondary motor area layer 5

PB Phosphate buffer

PD Parkinson's disease

PnO Nucleus pontis oralis

PPN Pedunculopontine nucleus

PRF Pontine reticular formation

RBP4 Retinol binding protein 4

RF Reticular formation

RFP Red fluorescent protein

ROI Region of interest

SI Substantia innominate

SMT Simple Mouse Tracker

SNr Substantia nigra pars reticulata

TBS Tris-buffered saline

vGAT Vesicular GABA transporter

vGlut2 Vesicular glutamate transporter 2

1. Introduction

1.1. GENERAL INTRODUCTION

Adaptive and flexible behavior depends on the precise coordination of movement initiation and termination [1,2]. This process relies on synchronized interactions among various cortical and subcortical structures, including the neocortex, basal ganglia (BG), brainstem, thalamus, and cerebellum. Among these, the thalamus plays a vital role in integrating motor inputs and coordinating the effects of subcortical structures on the neocortex [1–5].

The BG plays a crucial role in planning, executing, and learning complex motor sequences, making it one of the most extensively researched motor-related systems. A defining characteristic of the BG system is its organization into multiple embedded loops, which involve complex interactions between the cortex, BG, and thalamus, creating a hierarchical structure of nested circuits [6–8].

The concept of multiple nested loops in the nervous system refers to interconnected pathways that enable bidirectional communication between brain regions [9–11]. In the cortex-BG-thalamus system, signals travel through both direct and indirect routes, ensuring coordinated processing [6–8]. The direct thalamo-cortical pathway conveys information rapidly from the thalamus to the cortex, while the indirect pathway involves BG processing before returning signals to both the thalamus and cortex. This dual transmission system facilitates the integration and refinement of motor commands.

The strong topographical organization of these pathways ensures that the direct and indirect signals converge in the same thalamic regions, specifically within the intralaminar and parafascicular complex (IL/Pf) [7,8,12]. Individual cortical neurons can send axon collaterals to both the direct thalamo-cortical pathway and the indirect BG-thalamus-cortex loop [13–15]. This organization ensures that identical cortical messages are propagated through both circuits, promoting robust signal transmission and adaptability. This connectivity pattern is particularly beneficial for generating multiple embedded rhythms, which are essential for coordinating locomotion and adaptive movement control [1].

Another key feature of the BG is its influence extending beyond the cortico-BG-thalamocortical loop (C-BG-T) to brainstem structures [16,17]. Recent research has highlighted how BG outputs affect various regions of the brainstem, including one of the most important targets of BG, the pontine reticular formation (PRF)[16,17]. These data show that the substantia nigra pars reticulata (SNr), a key BG output nucleus, selectively inhibits excitatory neurons containing vesicular glutamate transporter 2 (vGlut2) within the PRF. These PRF/vGlut2+ neurons project to the contralateral gigantocellular nucleus (Gi) in the lower brainstem. Gi is known to be involved in executing appropriate motor commands via the spinal cord [17]. Additionally, it has been demonstrated that the secondary motor (M2) and cingulate (Cg) cortices project to the PRF (18).

The experiments demonstrated that reduced inhibitory BG output increased the activity in PRF/vGlut2+ neurons. As a consequence, contralateral Gi activity was enhanced, which promoted turning movement toward the side opposite to the BG-PRF interaction [17–19]. Conversely, increased BG output suppresses this activity. Moreover, modulation of the PRF/vGlut2+-Gi pathway could restore turning ability after striatal damage, indicating that disruptions in this pathway may contribute to turning deficits observed in the Parkinson's disease (PD) model in mice [17]. These findings illustrate how outputs of the BG loop can directly influence behavior by altering brainstem motor center activity.

In the PRF, in addition to excitatory neurons, there is also an inhibitory population expressing glycine transporter 2 (PRF/GlyT2+ cells) [20]. Interestingly, BG output apparently did not directly affect this other major PRF cell type. PRF/GlyT2+ neurons exhibit a dual GABAergic/glycinergic phenotype and project to the IL/Pf thalamic regions [17,20–22].

Due to its extensive connectivity, the IL/Pf is well-positioned to regulate adaptive movement and behavioral flexibility [23–26]. It integrates substantial input from the brainstem and maintains extensive reciprocal connections with higher-order motor-related cortical areas, including the M2/Cg and the frontal cortex. Additionally, it receives input from both the BG and cerebellum, contributing to its role in motor control networks and innervating the striatum [27–31].

During my PhD work, we examined the role of inhibitory PRF/GlyT2+ neurons as part of a cortico-subcortical-thalamus nested loop and their influence on motor behavior. We

described a cortico-PRF-thalamic loop (C-PRF-T), in which M2/Cg project to PRF/GlyT2+ neurons [32], which in turn, inhibit the ipsilateral IL/Pf and thereby modulate contralateral turning behavior. Although the PRF circuit operates in parallel with the BG loops, the BG and PRF influence on the thalamus is integrated via their convergence in IL/Pf, offering a novel perspective on adaptive motor control.

1.2. THEORETICAL BACKGROUND

1.2.1. Basal ganglia loops

The cortico-basal ganglia—thalamocortical (C-BG-T) loop is a fundamental network motif in the brain, classically conceptualised to contain three information channels: motor, limbic, and associative [6,7,33]. It involves the cortex, BG (striatum, globus pallidus, substantia nigra), and thalamus (Figure 1A) [6,34]. The striatum, as the input side of the BG, receives projections from virtually all areas of the cerebral cortex and the limbic system [6,7,33]. These cortical inputs are topographically organised, segregating into distinct streams (cognitive, sensorimotor, limbic) that project to appropriate zones of the striatum.

This topography is largely preserved through downstream projections from the striatum to the globus pallidus interna (GPi) and SNr, and various thalamic nuclei, maintaining segregated and independent loops (Figure 1A) [6,7,34]. The loop includes direct (striatonigral) and indirect (striatopallidal) pathways, both of which ultimately converge onto the same postsynaptic SNr neurons (Figure 1A) [7]. The BG outputs, primarily from the SNr and GPi, send large multisynaptic inhibitory terminals that innervate the thalamus (ventromedial and IL/Pf), while the thalamocortical cells close the C-BG-T loop (Figure 1A) [7,34].

The C-BG-T loops are critical for regulating motor functions, action selection, and maintaining concurrent goals [7,33]. They are implicated in motor planning, mapping sensory cues to actions, integrating spatial information, and supporting goal-directed behaviour [33]. Distinct functional domains within the striatum, based on converging cortical and thalamic projections, form subnetworks that are preserved through the pallidal/nigral and thalamic nodes, returning as parallel closed-loop circuits to the cortex where the corticostriatal neurons are found [7,33,34].

The IL/Pf thalamus acts as a central hub in C-BG-T loop, which integrates subcortical outputs and selectively routes them to different cortical targets, thereby allowing information from one loop (e.g., limbic) to influence another (e.g., motor) [34,35]. Dysfunctions in the specific subnetworks of the C-BG-T network are believed to underpin complex neurological and neuropsychiatric disorders, including PD. In PD, aberrant discharge patterns and exaggerated oscillatory activity are observed within these circuits, particularly in the Pf and motor cortex [7,34,35].

PD is a progressive neurodegenerative disorder, characterized primarily by the selective degeneration of dopaminergic neurons in the midbrain substantia nigra pars compacta (SNc) [36,37]. As a result, dopamine levels in the striatum decline; the striatum, as the main input region of the BG, plays a key role in the processes of motor planning and initiation. Dopamine depletion disrupts the delicate balance between the so-called direct and indirect motor pathways, leading to bradykinesia, rigidity, tremor, and postural instability. The toxin-based 6-hydroxydopamine (6-OHDA) PD mouse model enables the selective investigation of dopamine-deficient states, allowing experimental investigation of the C-BG-T loops.

1.2.2. Reticular formation

The reticular formation (RF), particularly the pontine reticular formation (PRF) and medullary reticular formation, constitutes a critical brainstem network involved in regulating movement and locomotion [2,38]. Originally the ascending reticular activating system (ARAS), arising also from the RF, was considered to be one of the most crucial systems responsible for maintaining and regulating the alternation between sleep and wakefulness [39].

The RF, via its thalamocortical connections, plays a key role in shaping the current level of arousal [39,40] by eliciting the switch between high-amplitude, low-frequency oscillations, characteristic of resting or sleep states, and the low-amplitude, high-frequency EEG signals observed during wakefulness. This was first demonstrated by Moruzzi and Magoun, who in 1949 electrically activated the RF in anesthetized animals, which resulted in the desynchronization of cortical slow-wave activity and the emergence of an EEG pattern characteristic of wakefulness [41]. These findings have since been supported by single-unit recordings from the RF, which reveal higher frequency firing

patterns during wakefulness [40]. Furthermore, increased single-neuron activity in the RF often precedes state transitions in the cortex, suggesting that its depolarizing influence may indeed contribute to the initiation of wakeful states [40]. Taken together, these findings suggest that the RF exerts regulatory control over cortical activity, thereby modulating levels of consciousness and arousal.

As mentioned above, the RF is also an integral part of the brainstem locomotor circuitry [1,2]. The mesencephalic locomotor region (MLR) - including the cuneiform nucleus (CnF) and pedunculopontine nucleus (PPN) – can activate neurons in the medulla that project to spinal locomotor centers via the ventrolateral funiculus (Figure 1B-C) [2,38]. Among these, the lateral paragigantocellular nucleus (LPGi) emerges as a key target of MLR input, receiving convergent glutamatergic signals, specifically from vGlut2-expressing MLR neurons [1,2]. These excitatory neurons also innervate other medullary subregions, including the gigantocellular nucleus (Gi) and its subdivisions. Optogenetic activation of vGlut2+ neurons in the LPGi reliably initiates locomotion [2,17,19].

The reticulospinal system also fine-tunes motor commands through bilateral or often asymmetric descending projections, including crossed modulation of hindlimb motor neurons [2,17,19,38]. Within this network, glutamatergic Chx10+ neurons in the Gi are crucial for shaping locomotor rhythm and mediating gait asymmetry during directional changes (Figure 1D) [18]. These neurons form a prominent ipsilateral descending tract targeting the spinal cord, situated at the level of the pyramidal decussation [2,17,38].

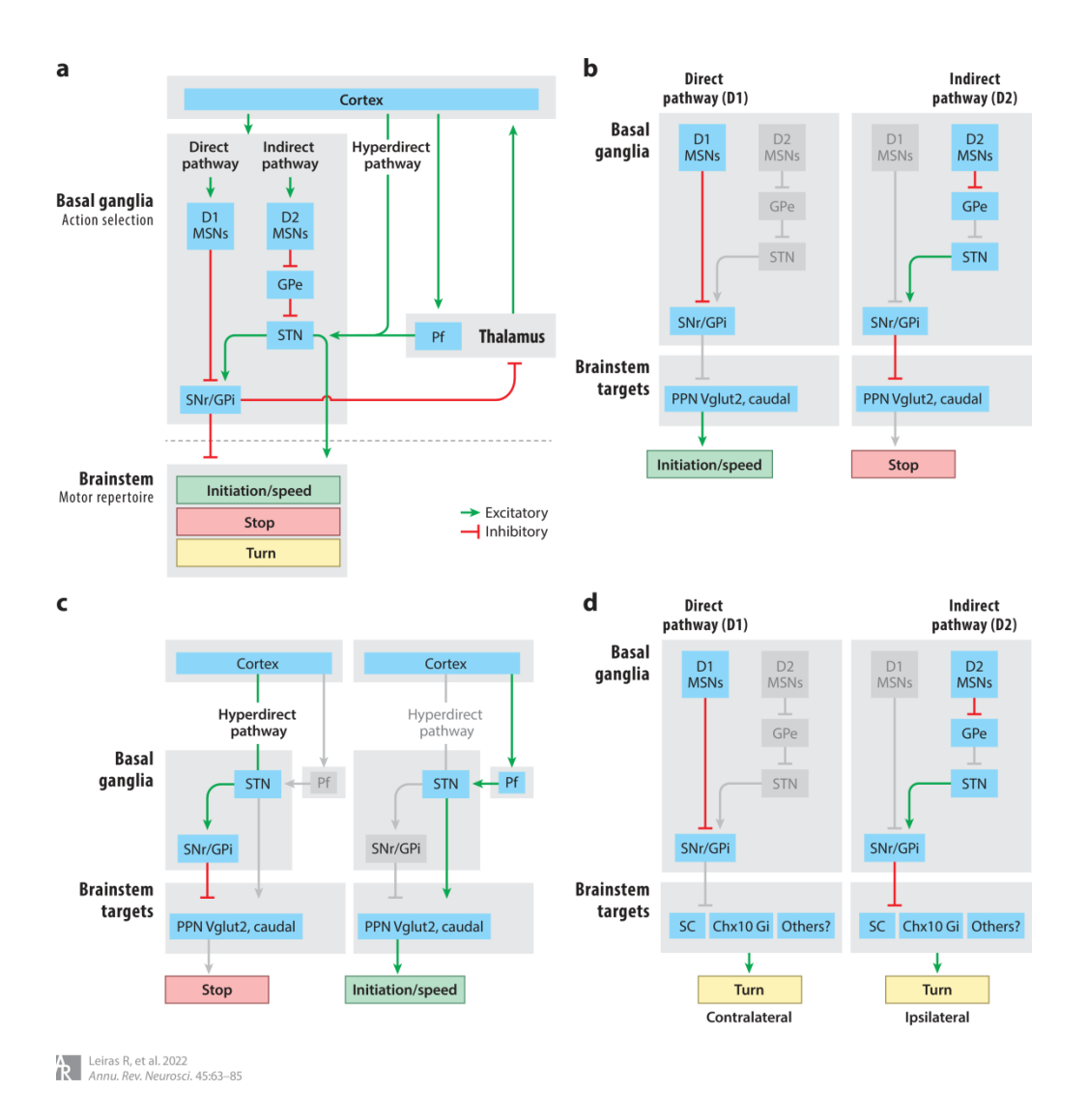


Figure 1) Basal ganglia loops and brainstem targets

A) Simplified C-BG-T loop diagram. C-BG-T pathways convey identical cortical signals via distinct routes, converging in the IL/Pf to integrate and refine motor commands. This organization supports rhythmic coordination of movement and extends beyond cortical loops to influence brainstem targets. **B)** Locomotion control via MLR (PPN). **C)** Locomotion control via STN pathways. **D)** Turning control. Turning is thought to be mediated by SNr inhibition of brainstem motor circuits, potentially involving Chx10 Gi neurons, the superior colliculus (SC), or other unidentified brainstem targets. The figure was adapted from a previously published source [2], therefore, its original formatting has been retained.

As mentioned before, the BG directly influences brainstem motor centers via projections from the SNr to the PPN, the CnF, and the PRF [1,2]. The PRF, which includes the nucleus pontis oralis (PnO) and nucleus pontis caudalis (PnC), is also involved in motor regulation [17,20]. A particularly important pathway for directional locomotion connects the SNr to the PnO/vGlut2+ neurons, then to Chx10+ Gi neurons, and ultimately to the

spinal cord [17]. Neurons in the PnO that receive input from the SNr are commissural, projecting across the midline to the contralateral Gi.

PnO/vGlut2+ neurons have been used to alleviate the symptoms in a rodent PD model (17). In this study, mice were subjected to unilateral administration of the catecholaminergic neurotoxin 6-OHDA into the dorsomedial striatum. This treatment leads to a loss of dopaminergic (tyrosine hydroxylase-positive, TH+) terminals in the striatum on the injected side and a reduction of dopaminergic cell bodies in the ipsilateral SNc. These 6-OHDA-lesioned mice exhibited a dominant ipsiversive turning preference in both acute (4-6 days post-injection) and chronic (15-19 days post-injection) lesion states [17]. However, when graded optogenetic stimulation (using Channelrhodopsin-2 (ChR2) at 5-40 Hz) was applied to PnO/vGlut2+ neurons on the lesioned side (in both acute and chronic hemi-parkinsonian mice), the ipsiversive turning bias was reversed, successfully restoring straight locomotion at lower frequencies (5 Hz or 10 Hz). Higher frequencies (20 Hz, 40 Hz) resulted in contraversive turning.

This study also found that chronic silencing of contralaterally projecting PnO/vGlut2+ neurons in normal, non-hemiparkinsonian mice caused strong ipsilateral turning, and affected mice could not complete contralateral turning mazes, indicating the necessity of this pathway for natural exploratory behavior [17]. The results suggest that modulation of the PnO could potentially serve as a target for deep brain stimulation aimed at alleviating turning disabilities clinically in PD [17].

1.2.3. Intralaminar and parafascicular thalamus

The IL/Pf is positioned as a central hub in nearly all motor, sensory, and associative circuits and is well-placed to regulate circuit-wide neuronal activities [33,34,42–44]. Both in humans and rodents, the IL nuclei are classically subdivided into a rostral (anterior) and a caudal (posterior) group [29,45] but it is important to note that anatomical descriptions and delineations of these nuclei in the thalamus can be heterogeneous, and nomenclature varies between stereotactic atlases.

The rostral group includes the central lateral nucleus (CL), the paracentral (PC), and the centromedian nucleus (CM). And the caudal group, particularly relevant in the context of the BG circuitry, is the parafascicular nucleus (Pf).[29,33]. In the literature, IL sometimes

refers only to the rostral part of the IL. Therefore, I will use the term IL/PF to clearly indicate both the rostral and caudal parts. The IL-Pf complex has extensive cortical and subcortical connections, making it ideally poised to influence BG and cortical motor functions [3,8,43]. It receives diverse excitatory and inhibitory inputs from regions such as the zona incerta, reticular thalamus, internal globus pallidus (GPi), SNr, superior colliculus, and several brainstem areas, including the PPN, and from glycinergic neurons located in the PRF [20,22,31,46–50]. Other inputs include ascending pain pathways from the spinal cord and the brainstem, as well as projections from the cerebellum. Its main outputs are directed towards the striatum and various cortical areas, including motor cortices, Cg, M2, and frontal cortex. It forms a strategic node between ascending information from the spinal cord and brainstem, and forebrain circuitry involving the cerebral cortex and BG.

The projections from the CM and Pf together innervate most of the striatum in primates and rodents [3,44,45]. According to conventional models, the IL is considered a functional extension of the ARAS, serving as a relay through which the RF supports cortical coordination and the maintenance of consciousness during wakefulness [39,46].

The IL nuclei are sometimes referred to as the "gateway to consciousness" and are considered critical for the emergence of consciousness, with the intralaminar and medial nuclei (imTha) potentially acting as gates to modulate cortical activity and broadcasting information [47,48,51]. In early experiments, Hunter and Jasper electrically stimulated the imTha in freely moving cats [46]. Stimulation evoked cortical EEG patterns resembling human seizures, and they exhibited significantly reduced, sometimes completely inhibited, motor activity or turning behavior. These findings suggest that the RF affects cortical activity and motor output via the imTha, thereby influencing both arousal and movement.

In addition to animal studies, human case reports have also contributed to our understanding. For instance, Karen Ann Quinlan experienced a temporary cardiopulmonary arrest at the age of 21 and, following resuscitation, remained in a persistent vegetative state [48]. She lost consciousness, yet retained a partially preserved arousal and sleep-wake cycle. Postmortem examination revealed negligible cortical damage but significant lesions in the imTha.

One of the most recent studies showed that the imTha potentially act as gates to modulate cortical activity and broadcast information in humans [51]. The imTha activity precedes and predicts prefrontal cortex (PFC) activation in a conscious visual awareness task. Theta-band (2–8 Hz) oscillations in imTha drive cross-frequency coupling with PFC gamma activity, coordinating thalamofrontal loops. This direct thalamus-to-PFC information flow supports a model where consciousness emerges via thalamic regulation, challenging cortex-centered theories.

In a rodent study, many IL/Pf neurons were found to encode vector components of velocity, with distinct subpopulations tuned to ipsiversive or contraversive turning movements [23]. The firing of these velocity-sensitive neurons often preceded behavioral change, indicating a potential causal role in initiating and guiding orienting behavior. Optogenetic activation of vGlut2-positive Pf neurons elicited ipsilateral head or body turning, while inhibition produced behavioral arrest or downward head movements, supporting a model in which the Pf dynamically adjusts motor output by environmental demands [23].

IL/Pf have also been implicated in the construction of internal state representations, integrating motor information with attentional and contextual cues to support action selection [52]. This effect is likely mediated by thalamic inputs to striatal cholinergic interneurons, which are themselves critical for learning and flexible action control.

The IL/Pf complex is particularly significant in the pathophysiology of PD and related motor deficits [53–56]. Neuropathological studies have demonstrated selective neuronal loss in the IL/Pf complex in PD patients, and electrophysiological recordings from animal models reveal abnormal low-frequency oscillations and reduced spontaneous activity in IL/Pf neurons following chronic dopamine depletion. These changes are accompanied by excessive phase-locking of IL/Pf firing to cortical beta oscillations during movement tasks, suggesting maladaptive synchrony within thalamocortical loops [35,53–56]. Aberrant communication between the Pf and the motor cortex may thus underlie hallmark motor symptoms of PD such as bradykinesia, rigidity, and postural instability. Furthermore, disruption of thalamostriatal input, particularly to striatal CINs, may contribute to the observed loss of behavioral flexibility, a core deficit in both clinical and experimental PD [35,53–56].

Given its broad connectivity and functional versatility, the IL/ Pf has been explored as a target for therapeutic intervention, including deep brain stimulation (DBS) [43,44]. While early clinical approaches involved lesioning the –IL/Pf to treat rigidity, modern DBS studies have evaluated its efficacy in reducing tremor, dyskinesias, or axial symptoms in PD. However, IL/Pf DBS is generally considered an adjunctive therapy, with subthalamic (STN) and pallidal (GPi) stimulation remaining the gold standards for core motor symptom relief. It remains unclear whether the modest benefits of IL/Pf DBS are due to direct modulation of thalamic function or indirect effects via current spread to neighboring regions such as the mediodorsal or ventral thalamus.

In sum, the IL/Pf complex is not a passive relay but an active computational node within the motor control hierarchy. By integrating diverse afferents and projecting to both cortical and subcortical effectors, it coordinates movement initiation, directionality, and action selection. These data suggest that the IL/Pf may play an important role in supporting conscious processing, attention, arousal, and motor control.

1.2.4. Inhibitory connections between PRF and IL/Pf

A fundamental component of this network is the PRF-IL/Pf inhibitory pathway, which plays a crucial role in modulating thalamic activity, movement execution, and cortical dynamics [20]. This pathway is evolutionarily conserved across species, including rodents and humans (18).

PRF inhibitory neurons target the IL/Pf complex via large, multisynaptic inhibitory terminals and innervate large-caliber, proximal dendrites, that allows highly effective synaptic inhibition [20]. PRF inhibitory neurons display a dual GABAergic/glycinergic phenotype. The postsynaptic IL/Pf cells exhibit mixed GABAergic/glycinergic inhibitory postsynaptic currents (IPSC) upon the stimulation of PRF/GlyT2+ axons, depending on the composition of GABA_A and glycine receptors [20]. The receptor profile, particularly the balance between GABA_A and glycine receptors (GlyRs), determines IPSC kinetics, influencing the duration of inhibition within the IL/Pf and shaping thalamocortical output [20].

In vivo juxtacellular recordings in the IL/Pf reveal that optogenetic activation of PRF/GlyT2+ fibers leads to robust inhibition of IL/Pf neurons [32]. This inhibition

manifests as tonic suppression, characterized by a gradual reduction in firing rate, or phasic inhibition, marked by a brief cessation of activity following stimulation onset. The phasic inhibition displays kinetics consistent with fast GABAergic/glycinergic IPSCs observed in vitro [20,32]. Control neurons outside the PRF/GlyT2+ projection zone within the thalamus remain unaffected by stimulation, underscoring the specificity of this pathway.

The profound effect on the activity of PRF/GlyT2+ cells was paralleled by strong behavioral consequences: the activation of PRF inhibitory axons within the thalamus halted movement, induced behavioral arrest, and enhanced low-frequency cortical oscillations (1-6 Hz) [20]. Freely moving animals exhibit a significant (~30%) reduction in locomotion during stimulation, with higher-intensity activation leading to full behavioral arrest. These findings highlight the PRF-IL/Pf pathway as a critical component in movement regulation, integrating brainstem inhibition with thalamocortical dynamics.

Earlier data clearly demonstrated that both the PRF and IL/Pf receive cortical feedback. It is still unclear, however, how the PRF-IL/Pf pathway is regulated by the cortical inputs and whether the cortex-PRF-IL/Pf circuit fulfills the criteria of a multiple nested loop. The direct behavioral consequences of modulating the PRF/GlyT2+ cells are also unknown, and it remains to be investigated what other brain regions IL/Pf projecting PRF/GlyT2+ cells innervate.

2. OBJECTIVES

Given the critical interactions between the PRF and thalamus in movement regulation and the PRF's involvement in motor control, this study aims to determine whether thalamic-projecting PRF/GlyT2+ neurons contribute to a brainstem movement control system that interacts with the cortex and thalamus in nested loops. To this end, the specific objectives are as follows:

- To investigate the cortical afferents to PRF/GlyT2+ neurons, specifically focusing on the M2 cortical area's projection to the PRF, its cell type selectivity, topography and and exact innervation pattern.
- 2. To perform ultrastructural characterization of axon terminals on PRF/GlyT2+ somata and dendrites, including those originating from cortical neurons.
- To determine whether thalamus-projecting PRF/GlyT2+ cells participate in cortex– PRF-thalamus embedded loops and to identify additional projection targets of thalamus-innervating PRF/GlyT2+ neurons.
- 4. To examine the behavioural effects of selective, bidirectional, optogenetic modulation of PRF GlyT2+ cells.
- 5. To analyse the electrophysiological properties of M2/Cg cortex Layer 5 neurons.

Together, these objectives aim to elucidate how inhibitory brainstem neurons contribute to the organization of cortical motor outputs and the coordination of complex motor behaviors through thalamic and subcortical pathways.

3. Methods

3.1. Animal housing

All experimental procedures were approved by the Institutional Ethical Codex, Hungarian Act of Animal Care and Experimentation (1998, XXVIII, section 243/1998) and the Institutional Animal Care and Use Committee of the Institute of Experimental Medicine, Hungarian Research Network, Budapest and by the regulations of the European Union guidelines (directive 2010/63/EU). The experiments were performed by the National Animal Research Authorities of Hungary (PE/EA/877-7/2020). We used healthy adult male mice (40-150 days) for the experiments. We used the following mice strains: Thy-Chr2-EGFP, GlyT2-Cre (Tg) - B6129F1 and Bl6Fx, Rbp4/cre//BAC_glyt2/GFP (TgTg) - C57Bl/6J, vGAT/t2A-Flpo//BAC-vGlut2/icre (TmTg)-C57Bl/6J, BAC_glyt2/GFP - C57Bl/6J²⁹. Mice were entrained in a 12-hour light/dark cycle with food and water available *ad libitum*. We performed animal research according to the 3R principles.

3.2. Surgeries

3.2.1. Anesthesia

The surgeries were done for all experiments (anatomy, electrophysiology, optogenetics) based on the following protocol. As anesthetics, mice received an intraperitoneal injection of ketamine (111 mg/kg, Produlab Pharma, #07/01/2302) and xylazine (4.3 mg/kg, Produlab Pharma, #07/03/2303). For the maintenance of anesthesia, An intramuscular injection of ketamine/xylazine was administered every 30 to 50 minutes throughout the experiments. The animal's head was secured in a stereotaxic apparatus (David Kopf Instruments, Tujunga, California 91042, Model 900 Small Animal Stereotaxic Instrument).

3.2.2. Virus injections and fiber-optic implantations

For the anatomical investigations, all stereotaxic tracer injections were performed using a glass pipette (intraMARK, 20-30-µm tip diameter, BLAUBRAND, injection flow: 25nl/min) connected to a syringe and a stereotaxic micromanipulator (Kopf Instruments). After the injection, the capillary was left at the injection site for 5 to 10 minutes before

slow withdrawal to allow diffusion and minimize backflow. The mice were perfused or were used for experiments following a 3–6-week survival time.

For the investigation of the cortico L5-PRF pathway, we used Rbp4/cre//BAC_glyt2/GFP (TgTg) mouse line (altogether n=11 mice). We injected AAV5.EF1.dflox.hChR2(H134R)-mCherry.WPRE.hGH (based on Addgene plasmid #20297, UNC Vector Core) cre-dependent virus into the frontal cortex, M2/Cg (AP: Br.1 mm and 2 mm; ML: Br.0.5 mm; DV: 0.7 mm; bilaterally into 2-2 AP position, 80 nl each, 4 injection sites/mouse).

For labeling the axon collaterals of IL/PF targeting L5 neurons, we used two types of virus injection design (n=4), where in two cases we injected AAVrg-EF1a-DIO-FlpO-WPRE-HGHpA (Addgene #87306-AAVrg) virus into the Pf unilaterally (AP: -2, ML: 0,5, DV: 3; 30 nl). After three weeks, we injected AAV2/1-EF1a-fDIO-mCherry (Addgene #114471-AAV2) virus into the M2/Cg (AP: Br.1 mm and 2 mm; ML: Br.0.5 mm; DV: 0.7 mm; unilaterally into 2 AP positions, 80 nl each, 2 injection sites/mouse).

The other two cases we used BAC_glyt2/gfp mouse line (n=2), and we injected AAVrg-EF1a-Cre (Addgene # 55636-AAVrg) into the Pf unilaterally (AP: -2, ML: 0,5, DV: 3; 30 nl). We waited three weeks and injected AAV5.EF1.dflox.hChR2(H134R)-mCherry.WPRE.hGH (based on Addgene plasmid #20297, UNC Vector Core) into the M2 (AP: Br.1 mm and 2 mm; ML: Br.0.5 mm; DV: 0.7 mm; unilaterally into 2 AP positions, 80 nl each, 2 injections/mouse).

The last experimental design of the cortico L5-PRF pathway's investigation was labeling M2 axons on Pf-projecting PRF/GlyT+ neurons in GlyT2-Cre mice (n=4). We injected AAV5-CAMKIIa-CHR2(H134R)-EYFP (Addgene #26969-AAV5) into the M2 (AP: Br.1 mm and 2 mm; ML: Br.0.5 mm; DV: 0.7 mm; unilaterally into 2 AP positions, 80 nl each, 2 injection/mouse) and AAVrg-hSyn-DIO-mCherry (Addgene #50459-AAVrg) into Pf unilaterally (AP: -2, ML: 0,5, DV: 3; 30 nl).

For the investigation of the PRF/GlyT2+-thalamic pathways altogether, n=20 adult GlyT2-Cre male mice were used, including the in vivo optogenetic behavioral (n=17), experiments and anatomical investigation (n=3). For optogenetic activation of PRF/GlyT2+ cells, we injected AAV5.EF1a.DIO.hChR2(H134R)-eYFP.WPRE.hGH (based on Addgene plasmid #20298, UNC Vector Core). For optogenetic activation of

PRF/GlyT2+ fibers in the IL/Pf, we did the same injections but bilaterally. For optogenetic inhibition of the PRF/GlyT2+ somata, we injected AAV5-Ef1a-DIO eNpHR 3.0-EYFP (Addgene #26966-AAV5) into PRF bilaterally (AP:-4.4, ML:0.8, DV: 4.2, 100-100 nl). In the control experiment, we injected AAV5.EF1a.DIO.eYFP.WPRE.hGH (based on Addgene plasmid #27056, Penn Core) virus into the PRF unilaterally (AP:-4.4, ML:0.8, DV: 4.2, 100 nl).

After virus injection the optic fibers (Thorlabs, FG105UCA, Ø105 μm core, 0.22 NA) were implanted into the PRF (n=15 optic fiber in n=11 mice, AP:-4.4, ML:0.8, DV: 4.2) or IL/Pf (n=7 optic fiber in n=2 mice, AP:-1.9 and 2.3 mm; ML: -0.8 mm; DV: -2.5 or -2.8 mm). Mice recovered from surgery and the viruses could transfect the PRF/GlyT2+ cells for 3 weeks before behavioral testing or juxtacellular recording. The optic fibers were labeled with DiI stain (1,1'-Dioctadecyl-3,3,3',3'-Tetramethylindocarbocyanine Perchlorate ('DiI'; DiIC18(3); ThermoFisher Scientific, #D282).

For further investigation of the PRF/GlyT2+-thalamic pathways, we labeled the axon arbors of PF targeting PRF/GlyT2+ cells (n=3 in GlyT2-Cre mice). We injected AAVrg-EF1a-DIO-FlpO-WPRE-HGHpA (Addgene #87306-AAVrg) virus into the Pf unilaterally (AP: -2, ML: 0,5, DV: 3; 30 nl). After three weeks we injected AAV1-EF1a-fDIO-EYFP (Addgene #55641-AAV1) or AAV1-Ef1a-fDIO mCherry (Addgene #114471-AAV1) into PRF unilaterally (AP:-4.4, ML:0.8, DV: 4.2, 100 nl).

For examining PRF/vGlut2+ and PRF/vGAT+ projections in the Gi we used vGAT/t2A-Flpo//BAC-vGGlut2/icre mice (n=3). We injected mixed AAV5-hSyn-DIO-mCherry (Addgene #50459-AAV5) and AAVDJ-EF1a-fDIO-EYFP-WPRE viruses (based on Addgene plasmid #55641, UNC Vector Core) into the PRF unilaterally (AP:-4.4, ML:0.8, DV: 4.2, 100 nl; 1:1 ratio of the viruses).

3.3. HISTOLOGY

3.3.1. Perfusion and tissue fixation

Perfusions were performed under deep anesthesia (sodium pentobarbital 60 mg/kg). Using saline and a fixative solution (0.1% glutaraldehyde (wt/vol) (Electron Microscopy Sciences, #16210) and 4% paraformaldehyde (wt/vol) (TAAB Laboratory, #P001) in 0.1

PB. A peristaltic pump perfused the solutions through the ascending aorta. After fixation, the brain was sectioned into 50 µm coronal slices using a vibratome.

3.3.2. Immunohistochemistry

For all immunostaining methods, we used TBS buffer. The sections were incubated in sucrose solutions for cryoprotection and were frozen above liquid nitrogen to help the penetration of the antibodies, followed by BSA (bovine serum albumin) treatment (4% 40 min). To visualize the L5 fibers (ChR2-mCherry viral tracer) we used a rabbit anti-mCherry primary antibody (1:4000 or 1:1000, BioVision, Inc., 23 California 95035, #5993-100, overnight). To label GlyT2+ cells and fibers in the PRF and in the IL/Pf (in the case of eYFP containing viral tracers or in the Rbp4/cre//BAC_glyt2/GFP mouse line), the sections were treated with chicken anti-eGFP primary antibody (1:15000 or 1:1000, ThermoFisher, #A10262).

For light and electron microscopic analysis when we visualized the L5 fibers in the brainstem after the anti-mCherry primary antibody we used anti-rabbit ImmPRESS (1:2, Vector Laboratories Burlingame, Ca 94010) and DAB-Ni/DAB (DAB-Ni: Nickel-intensified 3,3'-diaminobenzidine (bluish-black reaction product), DAB: 3,3'-diaminobenzidine, Sigma-Aldrich, #D5637, brown reaction product) as a chromogen. In the other case, after the anti-eGFP primary antibody (1:15000, ThermoFisher, #A10262) we used ABC (avidin biotinylated horseradish peroxidase complex, 1:300, Vector Laboratories, #PK-4000) and DAB as a chromogen.

For fluorescent and confocal microscopic investigations of L5 fibers, after the antimCherry primary antibody, we used Cy3-conjugated goat anti-rabbit secondary antibody (1:500, Jackson Immunoresearch, RRID: AB_2313593; Code: 111-167-003) or Cy3-conjugated donkey anti-rabbit (1:500, Jackson Immunoresearch, RRID: AB_2307443; Code: 711-165-152). In the case of the anti-eGFP primary antibody, we used the anti-chicken-Alexa488 secondary antibody (1:500, ThermoFisher, #A-11039) or Alexa 488 donkey anti-chicken secondary antibody (1:500, Jackson Immunoresearch, RRID: AB_2340375; Code: 703-545-155) to investigate GlyT2//eGFP components.

After juxtacellular recordings, neurobiotin was visualized with Cy3-conjugated streptavidin (1:2000, Jackson Immunoresearch RRID: AB_2337244; Code: 016-160-

084) in the M2/Cg. To localize the fiber optics and juxtacellularly labeled cells, check virus injections, and analyze the fibers in the PRF, all micrographs were taken with OLYMPUS BX61, FLUOVIEW FV1000 confocal microscopy (software: Olympus Fluoview 1.6) or with ZEISS AxioPlan2 fluorescent microscopy with OLYMPUS DP70 camera (software: Olympus DPController 1.2.1.108) or Zeiss Axio Imager M1 microscope coupled to an AxioCam HrC digital camera.

3.4. MICROSCOPY

3.4.1. Fluorescent microscopy

To verify virus expression and optic fiber placement, fluorescent images were captured using a Panoramic Digital Slide Scanner (Zeiss, Plan-Apochromat 10X/NA 0.45, xy: 0.65 µm/pixel, Panoramic MIDI II; 3DHISTECH, Budapest, Hungary). Every sixth section was stained and analyzed for each animal. Axonal projections in the Gi originating from different cell populations in the PRF were quantified by delineating regions of interest (ROIs) in the Gi (ipsilateral and contralateral, each 0.25 mm²) based on neuroanatomical landmarks identified using Hoechst counterstaining on fluorescent images, which were delineated with SlideViewer software (3DHISTECH).

3.4.2. Confocal microscopy

Confocal images of the M2/Cg, IL/Pf, and PRF regions were captured using a Nikon C2 Confocal Laser Scanning Microscope. The imaging was performed with a 4x Plan Fluor objective (NA 0.13, xy resolution 2 μ m/pixel), a 10x Plan Fluor objective (NA 0.13, xy resolution 0.63 μ m/pixel, z-step size 2 μ m), and a 20x CFI Plan Apo VC objective (NA 0.75, xy resolution 0.32 μ m/pixel, z-step size 1 μ m, Nikon Europe). Confocal microscopy was used to analyze the spatial relationship between M2/Cg axonal boutons and labelled dendritic segments in the PRF. eYFP fluorescence was amplified using anti-GFP labelling, and for close apposition analysis, RFP fluorescence was amplified with anti-RFP labelling. To assess close appositions between axonal boutons and dendritic segments in the PRF, high-resolution z-stack images (Nikon CFI Plan Apo VC60X/NA 1.40 Oil objective, 0.09 μ m/pixel, z-step size 0.3 μ m) were taken from 5 μ m of the slice. Confocal images were acquired with consistent settings for pinhole size, gain level, axial

section depth, and laser intensity across all PRF slices. Close appositions, defined as potential synaptic contacts between labeled axonal boutons and dendritic segments, were manually quantified using NIS Elements Software. The analysis focused on identifying and counting instances where eYFP- or RFP-labeled boutons were in close proximity to EGFP- or RFP-labeled dendritic segments, indicating possible synaptic connections.

3.4.3. Electron microscopy

To analyze the M2/Cg terminals' ultrastructure, we performed immunostaining for the ChR2-mCherry viral tracer (DAB, as described above). To confirm the innervation of PRF/GlyT2+ neurons from M2/Cg, we performed double immunostaining for the ChR2-mCherry viral tracer (DAB-Ni) and GlyT2+//eGFP (DAB) and processed the material for EM. In our hands, the modified DAB-Ni precipitate in the axon terminals could be unambiguously differentiated from the end product of marble-like DAB.

After double immunohistochemistry of L5 terminals and PRF/GlyT2+ cells the sections were treated with OsO₄ (0.5%, vol/vol, with 7% sucrose for 40 min in 0.1 M PBS), followed by dehydration, sequential incubation in ethanol, uranile acetate, and acetonitrile for ultrastructural analysis. The dehydrated sections were embedded in Durcupan (Sigma Aldricht, #44610Aldrich). Blocks containing PRF were re-embedded and sectioned to ultrathin sections (60 nm thick) with an Ultramicrotome (EM UC6, Leica Biosystems). The dendrites and terminals (area, diameter) were measured in three non-consecutive sections in FIJI software⁶². The sections were examined using a HITACHI 7100 electron microscope; the electron micrographs were taken with a Megaview digital camera.

3.5. IN VIVO ELECTROPHYSIOLOGY

3.5.1. Cortical activation and LFP recording

For in vivo investigation of the L5 M2/Cg pyramidal neruons we activated them optogenetically in Thy-Chr2-EGFP mouse line. (Optical fibers (200 µm core diameter) were positioned over the exposed M2/Cg region. The laser beam was generated by a 473 nm laser (Thorlabs lasers). 10 laser pulses were applied, 5 ms long, 0,1-10 mW intensity, and were delivered at 1,10 and 20 Hz frequencies

To record cortical field potentials, bipolar LFP electrodes (FHC, resistance $\sim 1~M\Omega$) were implanted into the frontal cortex of mice (Bregma 1.7 mm; lateral -0.8 mm). The acquired signal was amplified and band-pass filtered: from 0.16 Hz to 5 kHz for LFP recordings and from 100 Hz to 5 kHz for multiunit activity (Supertech BioAmp, Supertech, Pécs, Hungary), with digitization occurring at 20 kHz (micro 1401 MkII, CED, Cambridge, UK).

3.5.2. Juxtacellular recording

M2/Cg single unit activity was recorded using glass microelectrodes (in vivo impedance ranging from 20-40 M Ω) crafted from borosilicate glass capillaries (1.5 mm outer diameter and inner diameters of 0.75 or 0.86, Sutter Instrument Co., Novato, CA, USA or WPI Inc., Sarasota, FL, USA). Electrodes were placed on the surface of the M2/Cg (AP: Br.. 1 mm and 2 mm; ML: Br.. 0.5 mm) using a piezoelectric microdrive (Burleigh 6000 ULN or ISS 8200, EXFO, Quebec City, Quebec, Canada). Neuronal signals were amplified. (Axoclamp 2B, Axon Instruments/Molecular Devices), followed by additional amplification and filtering between 0.16 Hz and 5 kHz using a signal conditioner (LinearAmp, Supertech), and then recorded with Spike2 5.0 (CED). The electrodes contained a solution of 0.5 M K+-acetate and 2% neurobiotin (Vector Laboratories, Burlingame). Juxtacellular labeling of the recorded neurons was done by filling the neurons with neurobiotin, as described in 37 .

After the experiments, the animal was perfused, and coronal sections were cut from the whole brain (3.1. Perfusion and tissue fixation). To visualize neurons filled with neurobiotin and to determine their eGFP content, we treated the sections as described in 3.2. Immunohistochemistry.

3.6. Janelia Mouse Light Neuron Browser

We analyzed single-cell reconstruction data of the Mouse Light Neuron Browser⁴⁰ (https://www.janelia.org/open-science/mouselight-neuronbrowser) by identifying PRF projecting M2/Cg L5 neurons. We selected neurons that have their soma in the M2 or Cg area and projected to the PRF. In the browser, we could set the threshold to the axonal projection, called the in the browser "axonal endpoint". We used 4 thresholds: >=10, 5-

10, 2-5, or 1. We always precisely checked the anatomical region to uniform terminology that we used during our research (Paxinos atlas vs Neuron Browser).

3.7. Behavior

After virus injection and optic fiber implantation (see above) the experimental protocol included handling (2 weeks), habituation (3 days), and the optogenetic experiment. The handling period started 1 week after the surgery. During the habituation, we placed the mouse in the experimental box and connected their optic fiber to a fiber optic patchcord (Thorlabs) and the patchcord cable (Thorlabs). The mice moved freely in the experimental box and got used to the new environment and the weight of the cable and the mouse was allowed to move passively. During the experiment phase, we photoactivated or inhibited the transfected PRF/GlyT2+ cells or their fibers in IL/Pf. The photoactivation was generated by a 473 nm DPSS laser (LRS-0473-PFM-00050-03, Laserglow Technologies, Toronto, Canada). The photoinhibition was generated by 589 nm DPSS laser (LRS-0589-GFF-00100-05, Laserglow Technologies, Toronto, Canada) The photostimulation trains were 10 s long, 5 ms light pulses at 40 Hz in PRF every 1 minute in 4 laser intensities (1, 5, 10, 15 mW). The photoinhibiton trains were 10s long, and continuous stimulation. We stimulated every condition (every optic fiber) 20 times (5-5-5-5 stimulation by intensities), and the experiment took about 30 min. During IL/Pf stimulation we used 30 Hz After the experiments, we perfused the animals and identified the location of the virus injection and the optic fibers post hoc (see Histology).

3.8. Analysis

3.8.1. Density mapping analysis

Following fluorescent immunostaining, we investigated the density of L5 fibers in the PRF (Figure 2-4). A map based on fiber density was created by FIJI software16[57]. A high-magnification confocal micrograph was taken about PRF/GlyT2+ cells and M2/Cg L5 fibers (20x, NA: 0.75). The pictures were converted to 8-bit in depth then the brightest pixels of single optical slices of the original image stacks were projected into one plane to depict all of the labeled bright structures. These maximum intensity projections were smoothed by a Gauss filter with a radius of 40 pixels then the pixels were ordered

according to their intensity values in 8 categories. The result is a pseudocolored, semiquantitative map of the fiber density that enables the localization of the highest fiber density areas in a given image.

3.8.2. Terminal analysis

To illustrate the size characteristics of the three terminal types observed in the electron microscope (Figure 8), we created histograms of terminal areas using 20 equal-width bins within a fixed x-axis range of 0–3 μ m². Raw frequencies in each bin were divided by the total number of observations and by the bin width, transforming the y-axis to represent probability density. This normalization ensures that the area under the histogram sums to 1, allowing comparison between groups of different sample sizes. The histograms were overlaid with kernel density estimate (KDE) curves to represent the smoothed distribution of values.

3.8.3. Axonal density analysis

For axonal density analysis on the confocal images, FIJI was used to split the color channels of each image into red, green, and blue (Figure 19). The relevant channel (red for RFP, green for eGFP) was converted to grayscale. Background noise was removed, and the 8-bit images were then converted to binary with a consistent threshold for the reporter protein (RFP or eGFP). This allowed for the precise calculation of axonal density within the selected regions. Axonal density in each image was calculated and expressed as the mean area percentage. To statistically compare the ipsilateral and contralateral axonal densities, the data were normalized to the ipsilateral side.

3.8.4. Analysis of juxtacellular recording

To evaluate the effect of photoactivation the first APs following each stimulus were detected in a 40 ms window. They were distributed around ~10 ms peak with variable spread. Only APs in the [25th percentile - 1.5*IQR, 75th percentile + 1.5*IQR] & AP time > 0 ms range were considered evoked response. APs occurring outside of this range were considered baseline firing activity and were excluded from further analysis.

Electrophysiological data were processed using Spike2 (v7.0, Cambridge Electronic Design). Custom-written and built-in MATLAB scripts (MathWorks) were used for spike

sorting, latency analysis, and curve fitting. Experiments were not conducted under blinded conditions. For each stimulation trial, action potential latency and firing probability were measured. Response probabilities were calculated as the number of evoked APs/number of stimuli. Population response probabilities were averaged across neurons.

3.8.5. Video analysis for behavior

To analyze the movements during the experiment, we used Simple Mouse Tracker (SMT) downloaded from GitHub. SMT is a video tracker software based on Open CV that runs on any platform that supports Python. It is designed to track the body, head, and tail coordinates (X, Y) of a single-colour mouse over a homogeneous color background. https://github.com/joseaccruz/SimpleMouseTracker

After cleaning the tracking data (removing noise, outliers, and missing data) the beforestimulus speed and rotation of the animals were compared to the during-stimulus and -in the rotation experiments- to the after-stimulus periods.

To get the speed of the animals the Euclidean distance of the center (body) points across every 5th frame was calculated and converted to mm (scaling factor: 1.6 mm/pixel). To get the rotation of the animal the signed angle of the body-head vector was calculated across every frame and the mean rotation angles across frames were plotted.

For traveled distance plots every 5th frame (data point) was used (25 fps, scale: 1.6 pixel/mm). We calculated distances and average speed (mm/sec) across every 5th frame. Speed (mm/sec) is averaged through the last second of the "before stimulus" category and the first second of the stimulus and the last 9 seconds of the stimulus. Speed "after stimulus" is not included.

For rotation, we plotted every frame (data point). To show the animal's movement trajectory during stimuli the head-center-tail body points were plotted, separately in non-stimulated and stimulated periods. We calculated vectors (based on head-body X-Y coordination) and measured the mean angle changes of every vector. After that, we multiplied that number with fps values and divided that number by 360 to get which is the mean rotation angle during 1 sec relative to one whole circle. That value was multiplied by 100 to obtain the percentage of rotation within 1 sec in relation to a complete

circle. The global angle threshold used in this file is 90. Greater rotation angles between consecutive frames are replaced by zero.

3.8.6. Statistics

In all behavioral experiments, mice were randomly assigned to groups. Data points from animals with misplaced viral infections were excluded from the analysis. The number of animals used in each experiment is specified in the respective figure legends. All data were checked for normality, and outliers were defined as values outside the range of Q1 - 3IQR and Q3 + 3IQR. All statistical analyses were performed using R Statistical Environment, Jamovi v 2.328, and Prism 8 software (GraphPad Software). For the juxtacellular analysis, statistical correlation between laser intensity and firing probability or latency was calculated using Spearman's correlation coefficient. Behavioral data were analyzed using Friedman ANOVA with the Durbin-Conover post-hoc test. Ipsilateral and contralateral axonal projection density were analyzed using a two-sided paired t-test. To statistically compare the three terminal groups, we first tested for normality using the Shapiro-Wilk test. After it failed, we employed the Kruskal-Wallis test along with the Dwass-Steel-Critchlow-Fligner comparisons.

3.9. Funding

ERC Advanced Grant FRONTHAL, 742595 (LA)

European Union project within the framework of the Artificial Intelligence National Laboratory RRF-2.3.1-21-2022-00004 (LA)

Hungarian Academy of Sciences – "Lendület" Program LP2023-2/2023 (LA)

4. RESULTS

4.1. M2/CINGULATE CORTICAL NEURONS INNERVATE PRF/GLYT2+ NEURONS

Classical retrograde (fluorogold) tracing has shown that the M2/Cg cortices project to the PRF, but the distribution of fibers and the specificity of the cell types involved remain unclear [20]. We aimed to investigate the afferent connections to PRF/Glyt2+ cells. To visualize cortical inputs to PRF/GlyT2+ neurons, we used anterograde virus-mediated tracing in RBP4-Cre//GlyT2-eGFP double transgenic mice (n=9). RBP4, a retinol binding protein, is known to be expressed in deep layer 5 (L5) pyramidal cells that project to subcortical targets [58]. Using the Cre-recombinant system, we expressed anterograde viruses to label the pathway originating from L5 pyramidal cells that project to the brainstem. In this transgenic strain, all glycinergic neurons in the brainstem expressed GFP, allowing for the visualization of these cells via green fluorescence [21].

We injected AAV5-DIO-ChR2-mCherry virus into the M2/Cg cortices, which were colorized to magenta to visualize the injection sites (Figure 2A-C). GlyT2+ cells were detected by the eGFP expression. Anterogradely labeled M2/Cg fibers formed a dense axon arbor throughout the entire rostral PRF (Figure 2D-F). The distribution of cortical afferents exhibited significant overlap with the PRF/GlyT2+ neurons (Figure 2D-F), though it was not homogeneous within the PRF. After conducting fluorescent immunostaining, we analyzed L5 fiber density in the PRF and created maximum intensity projections to visualize the fibers' distribution. We developed a distribution map that reflects the light intensity of the innervation in the PRF. The pseudocolored, semi-quantitative fiber density map allowed for the localization of the areas with the highest innervation, where greater fiber density is represented by lighter grey colors (details in Methods). The density map of cortical afferents revealed a dorsomedial to ventrolateral decrease in fiber density within the PRF/GlyT2+ zone (Figure 2G).

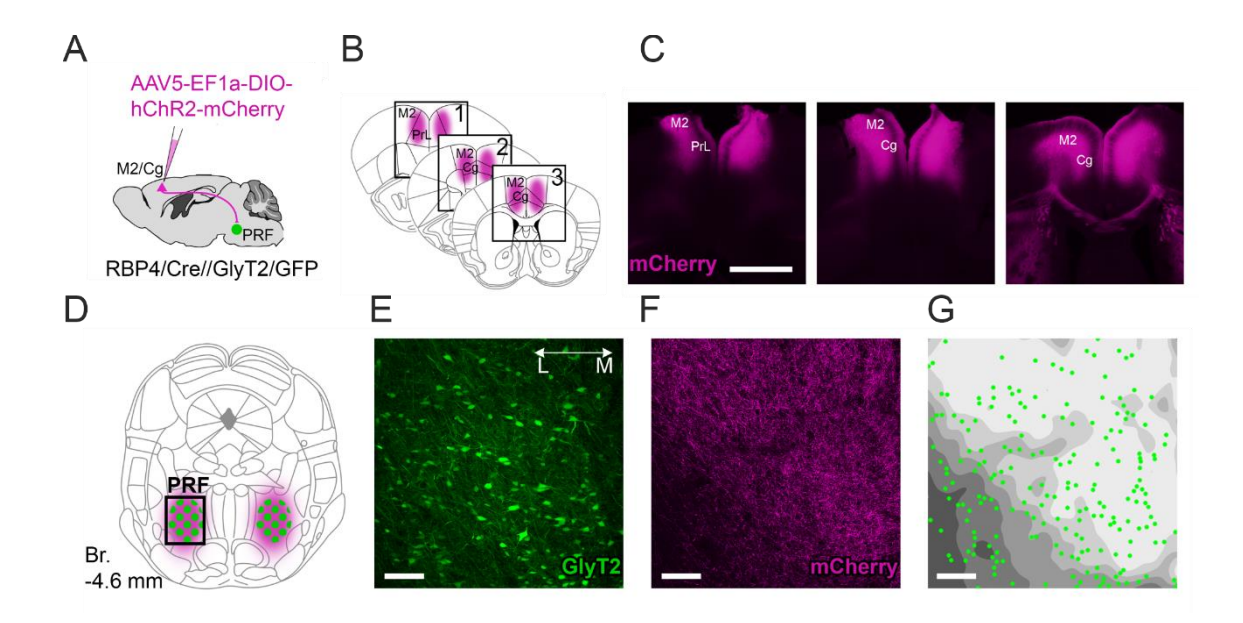


Figure 2) PRF/GlyT2+ cells surrounded by cortical terminals

A) Scheme of anterograde tracing from the frontal cortical motor-related areas (M2/Cg) in the RBP4-Cre//GlyT2-eGFP mouse line. **B**) Schematic view of the injection sites. **C**) Low-power fluorescent micrographs of the cortical injection sites at three anteroposterior levels. **D**) Schematic view of the M2/Cg fibers (magenta shade) and PRF/GlyT2+ cells (green dots). The black rectangle, the position of the micrographs and heatmaps in E-G. **E-F**) Confocal micrographs of the glycinergic cells (**E**) and anterogradely labeled M2/Cg cortical fibers (**F**) in the PRF glycinergic zone. **G**) Fiber density heat map showing the distribution of cortical fibers (grey shading) and PRF/GlyT2+ cells (green dots). Scale bars: C) 1 mm; E-G) 100 μm [32]

We investigated the fiber distribution through anteroposterior extension in three coronal slices, with a total thickness of approximately 250 microns. Intensity levels represent fiber density values ranging from 0 to 7, where 0 indicates no innervation and 7 represents the strongest innervation. Our data revealed a rostrocaudal increase in fiber density, with the highest axon density observed at Br. -4.84 (Figure 3A-C). Each coronal section exhibited the previously mentioned dorsomedial to ventrolateral decrease in fiber density (Figure 3A-C).

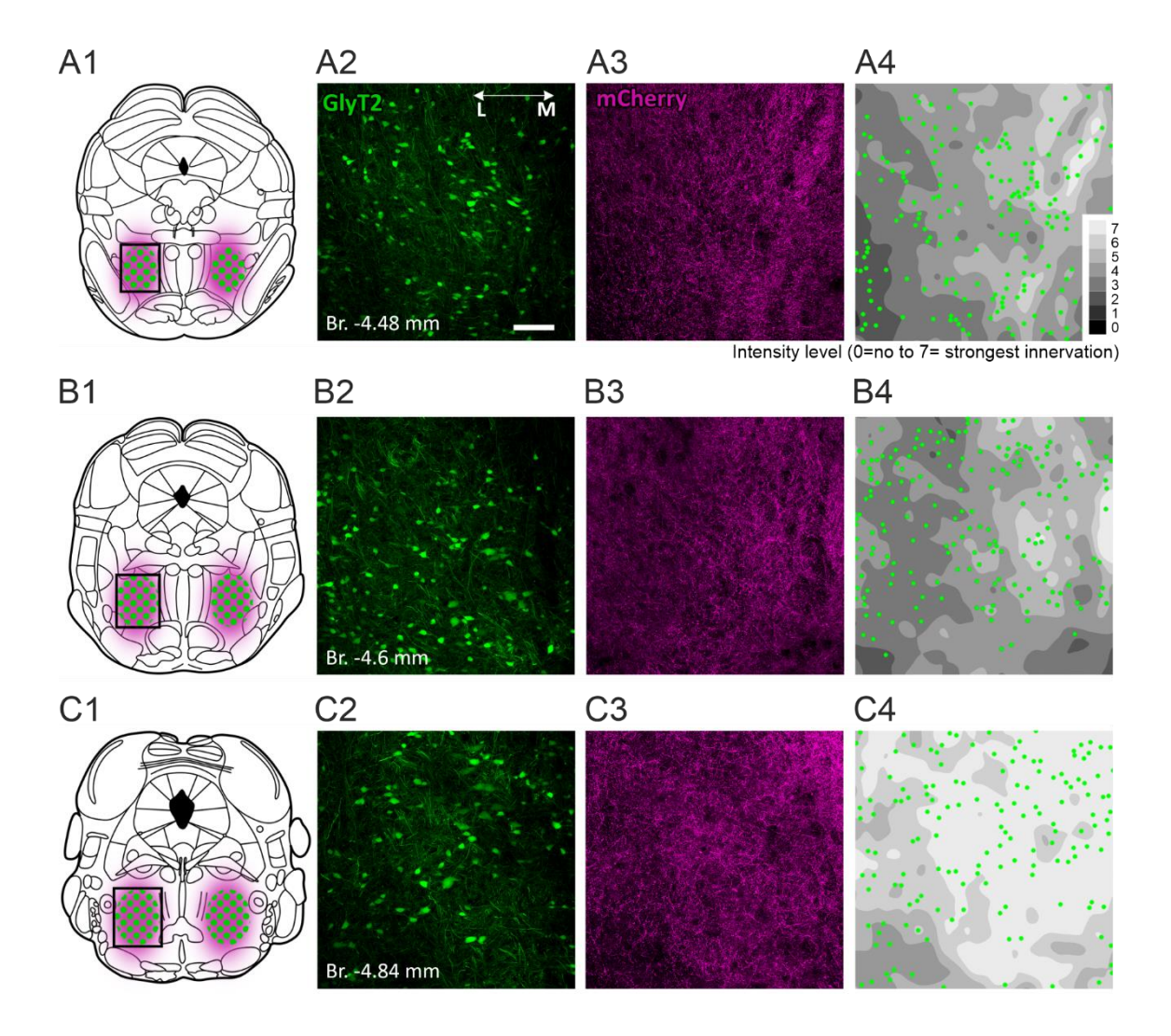


Figure 3) Anteroposterior PRF fiber mapping

A1) Schematic view of the M2/Cg L5 fibers (shaded magenta area) around the PRF/GlyT2+ cells (green dots). The black rectangle indicates the position of the micrographs and heatmaps in A2-4. **A2-3**) Confocal micrographs of the PRF/GlyT2+ cells (**A2**) and anterogradely labeled M2/Cg cortical fibers (**A3**) in a representative animal. **A4**) Fiber density heat map (grey shading) and PRF/GlyT2+ neurons (green dots) of the same region. Higher fiber density is indicated with light grey colors. **B-C**) As in **A**) at two more caudal levels. Scale bar: 100 μm. [32]

We averaged the density maps from three animals across the three displayed coronal levels, once again revealing the rostrocaudal increase in fiber density, with the highest axon density recorded at Br. -4.84 (Figures 4A1-3). Meanwhile, the density map resulting from more caudal (Br. 0) injections into the M2/Cg cortex (n=3) exhibited weaker PRF innervation (Figure 4B). Quantitative analysis of intensity levels indicated that the entire PRF received projections from M2/Cg (Figure 4C). The posterior M2/Cg afferents

showed low intensity levels (2-4) compared to the anterior M2/Cg innervation, which displayed higher fiber density, with intensity levels ranging from 1 to 7 (Figure 4D).

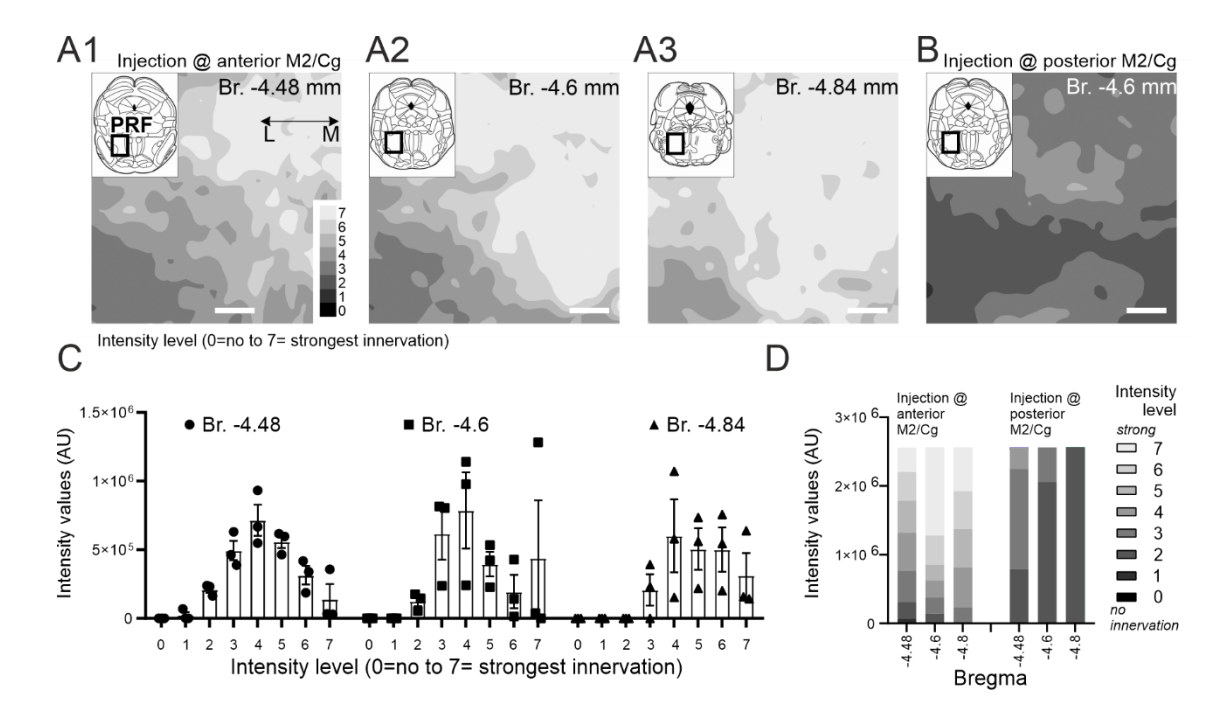


Figure 4) Averaged density maps and intensity levels

A1-3) Maximum intensity Z projections of average cortical fiber heat maps (n=3 animals) showing anterior M2/Cg inputs at three anteroposterior PRF levels extending from Br. -4.6 to Br. -4.84 (from the Paxinos atlas; 250μm) **B**) Maximum intensity Z projections of cortical fiber heat maps (n=3 animals) showing posterior M2/Cg inputs. **C**) Quantitative analysis of the anterior M2/Cg fibers in the PRF at three coronal levels. **D**) Proportion of innervation densities in the PRF after anterior (left) and posterior (right) M2/Cg injections at three coronal levels. Scale bars: A-B) 100 μm [32]

Next, we visualized the anterior M2/Cg fibers and PRF/GlyT2+ neurons using high-power confocal imaging and high-power light microscopy with DAB/Ni (black) and DAB (brown) chromogens. In both approaches, cortical afferents were frequently observed in close proximity to PRF/GlyT2+ elements (Figure 5A). Putative synaptic contacts were detected on the dendrites and, occasionally, on the somata of GlyT2+ neurons (Figure 5B, C). In one instance, the spine of a PRF/GlyT2+ neuron – labeled via the juxtacellular labeling method (see Methods) - was contacted by an M2/Cg cortical terminal (Figure 5D).

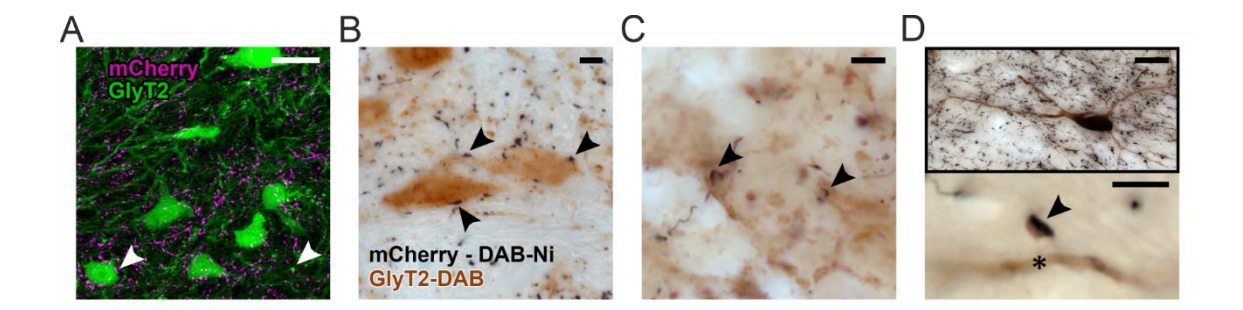


Figure 5) Close appositions between PRF/GlyT2+ elements and cortical terminals

A) High power confocal fluorescent image of anterogradely labeled M2/Cg fibers (magenta) and PRF/GlyT2+ neurons (60x, n=5 mice) **B-D**) High power light microscopic image (n=9 mice) of close apposition between M2/Cg fibers (black) and the somata (**B**), dendrites (**C**), or a spine (**D**) of PRF/GlyT2+ neurons. Inset in (**D**) displays the juxtacellularly labeled PRF/GlyT2+ cell; arrowheads, cortical inputs; asterisk, and spine. Scale bars: A) 20 μ m, B-D) 5 μ m and 20 μ m in the inset. [32]

Our results show that M2/Cg cortices project densely to the PRF, with increased fiber density rostrocaudally and significant overlap with PRF/GlyT2+ neurons. Cortical afferents also form putative synaptic contacts on GlyT2+ neurons, indicating functional interactions between these regions.

Chapter summary:

- ➤ The M2/Cg cortices project dense, anterogradely labeled fibers to the rostral PRF. These cortical afferents innervate the entire PRF/GlyT2+ zone.
- The maps show a decreased M2/Cg fiber density from dorsomedial to ventrolateral within the PRF/GlyT2+ area, alongside a rostrocaudal increase.
- The greatest axon density occurred at Br. -4.84, with the anterior M2/Cg cortex exhibiting a higher fiber density than the posterior M2/Cg cortex.
- ➤ High-power imaging revealed M2/Cg afferents near PRF/GlyT2+ neurons, showing putative synaptic contacts on dendrites, somata, and one spine.

4.2. ULTRASTRUCTURAL AND QUANTITATIVE COMPARISON OF SYNAPTIC TERMINALS IN THE PRF

Our next aim was to characterize the morphology and synaptic inputs of GlyT2+ neurons using electron microscopy (EM). Initially, we explored the ultrastructural features of M2/Cg terminals in the PRF without identifying their postsynaptic targets. Next, we analyzed the terminals on GlyT2+ somata and dendrites. Finally, we specifically focused on the synaptic contacts between M2/Cg terminals and GlyT2+ neurons.

We characterized M2/Cg terminals in the PRF with DAB visualization of the mCherry signal from M2/Cg axons (Figure 6A-C). Analyzing 34 PRF terminals revealed they were small to medium-sized, averaging 0.44 μ m² (SD = 0.29), with 1 to 3 mitochondria (Figures 6B-C). These terminals formed asymmetrical synapses with 1 to 2 active zones, primarily targeting dendrites measuring 0.197-1.437 μ m, averaging 0.59 μ m, with an SD of 0.33 (Figure 6B-C).

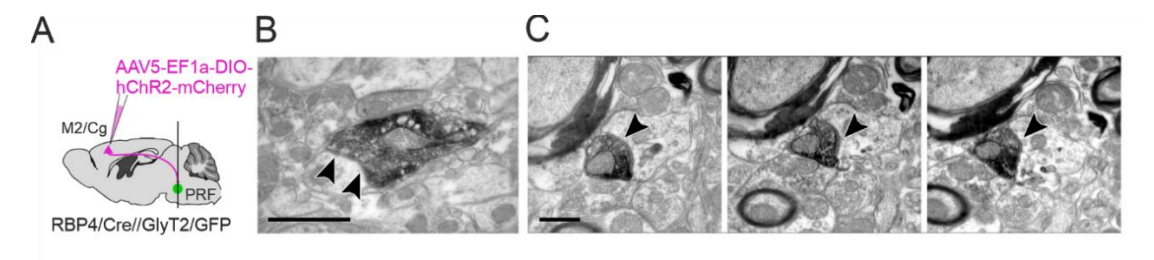


Figure 6) Ultrastructural characteristics of M2 and Cg terminals within the PRF

A) Scheme of anterograde tracing from the M2/Cg in the RBP4-Cre//GlyT2-eGFP mouse line The vertical line marks the area selected for ultrastructural analysis by electron microscopy **B-C**) Electron micrographs of M2/Cg terminals (n=34, dark precipitates) in the PRF contacting mid-caliber dendrites **C1-C3**) Serial EM images of the same axon terminal. Black arrowheads, synapses. Scale bars: B) 1000 nm C) 500 nm [32]

After, we used double immunostaining and labeled M2/Cg terminals with DAB-Ni and GlyT2+ elements with DAB. For the analysis of terminals on GlyT2+ somata, we used correlated sectioning in one representative case. After identifying GlyT2+ neurons based on brown DAB staining under a light microscope (Figure 7A), we re-embedded and sectioned the corresponding region for EM examination (Figure 7B). In this case, ultrastructural correlates of DAB-labeled GlyT2+ profiles were reliably identified. We measured three somata (two additional somata without correlated light microscopy) and identified and quantified 63 presynaptic terminals (mean area = $0.97 \,\mu\text{m}^2$ with SD = 0.66;

Figure 7C-D). These terminals were unlabeled; therefore, they did not originate from the virus-infected M2/Cg area and exhibited different ultrastructural properties. These larger terminals contained more than three mitochondria (Figure 7D). Typically, they displayed weak postsynaptic density (symmetrical synapse), suggesting that they may be large inhibitory terminals of unknown origin.

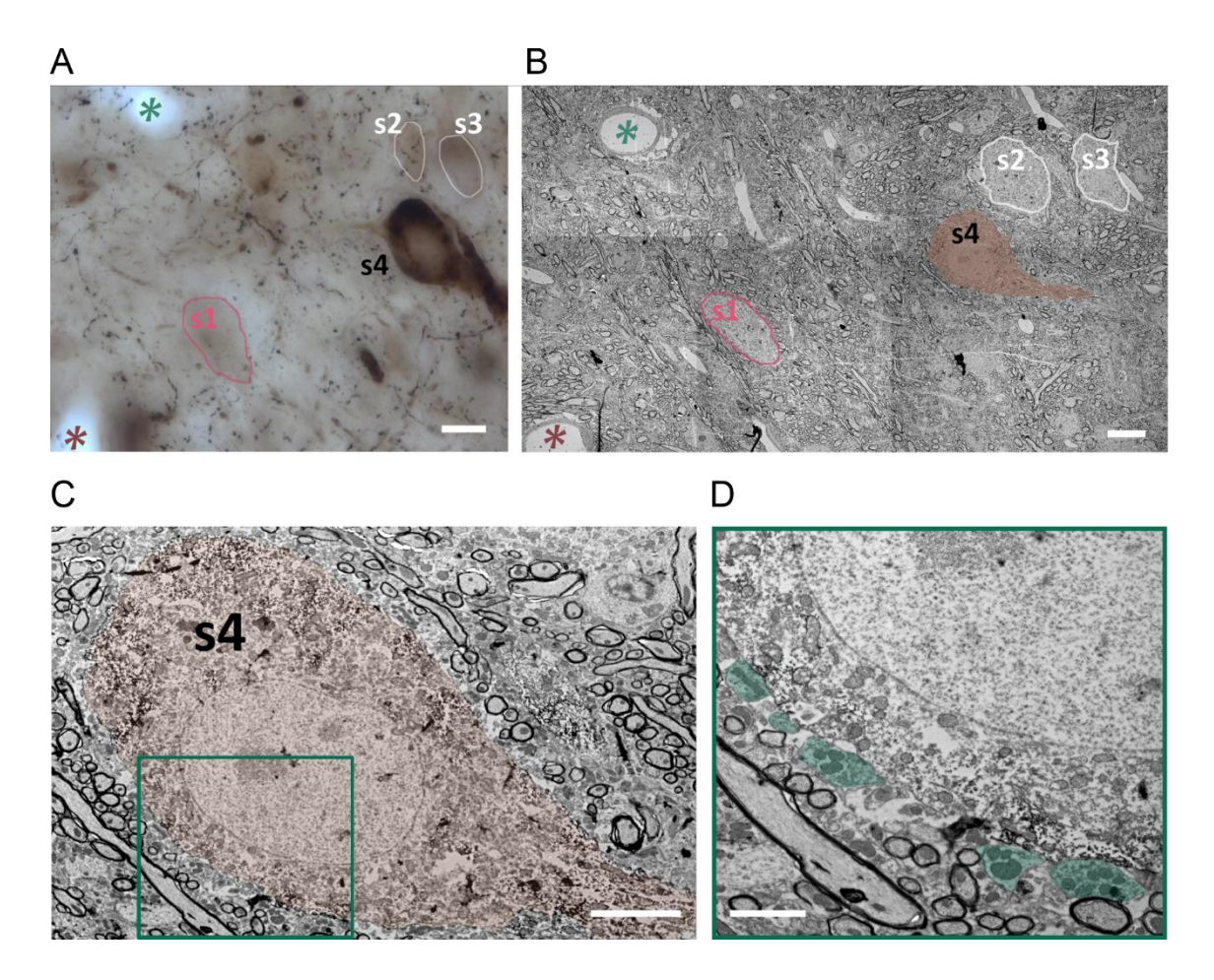


Figure 7) Large terminals contact PRF/Glyt2+ soma

A) Light microscopic and B) electron microscopic image of the same region. Identical colors indicate matching structures. C) The GlyT2+ neuron labeled s4 is shown at 3000× magnification. D) Presynaptic terminals (green) apposing the soma membrane within the boxed area. Note the DAB reaction product outlining the somatic profile. * - blood vessel, s1-4 – soma. Scale bars: A) 20 μ m, B) 10 μ m, C) 5 μ m, D) 1000 nm

For the analysis of GlyT2+ dendrites, we examined proximal dendritic segments (diameter ranging from 1393 to 5831 μ m) identified in the same electron microscopic dataset. We quantified 146 presynaptic terminals contacting 24 dendrites. The terminals

had a mean area of 0.64 μm^2 with a standard deviation of 0.39 μm^2 . None were DAB-Ni labeled.

We found synaptic connections between virus-labeled cortical afferents and PRF/GlyT2+ neurons in ten cases (see Figure 8A-D). In nine of these cases, the postsynaptic structure appeared as a mid-caliber dendrite, while in one case, it was a PRF/GlyT2+ spine. Their terminals had a mean area of $0.60 \, \mu m^2$ (SD = 0.37), and the diameter of the postsynaptic elements had a mean of $0.73 \, \mu m$ (SD = 0.26).

We statistically compared terminal sizes across the groups (M2/Cg terminals, non-M2/Cg on somata, and non-M2/Cg on proximal dendrites). All groups showed a non-normal distribution (Shapiro-Wilk p < 0.05); thus, we applied non-parametric tests for group comparisons. Descriptive statistics revealed that M2/Cg terminals had a median area of 0.37 μ m², dendrite-targeting terminals 0.54 μ m², and soma-targeting 0.79 μ m² (Figure 8E). A Kruskal–Wallis test revealed a significant effect of terminal type on area (χ^2 = 25.3, df = 2, p < 0.001, ε^2 = 0.100). Post hoc analysis using the Dwass–Steel–Critchlow–Fligner test showed that M2/Cg terminals were significantly smaller than non-M2/Cg terminals on both somata (p < 0.001) and dendrites (p = 0.003). Soma-targeting terminals were also significantly larger than dendrite-targeting ones (p = 0.003) (Figure 8E).

To further illustrate the distribution of terminal sizes, we plotted histograms for each group (Figure 8F–H). The distributions of terminals showed right-skewed patterns, although somatic terminals exhibited a broader range and a higher proportion of large terminals compared to other ones. M2/Cg terminals displayed the most compact distribution with the lowest average and median area.

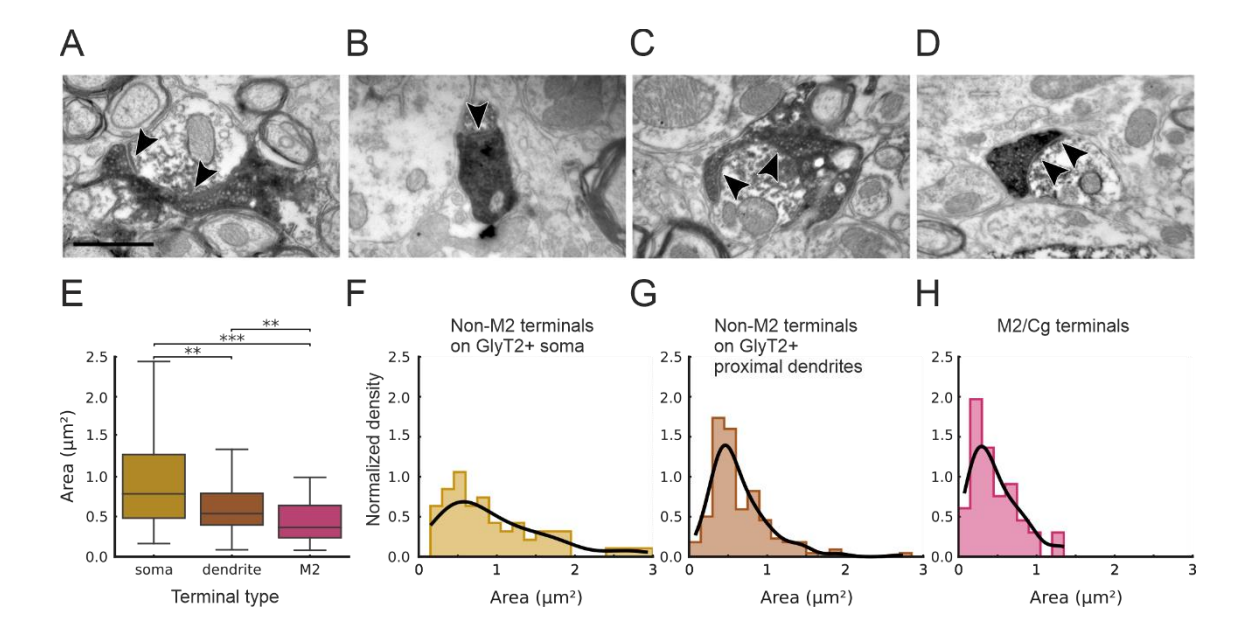


Figure 8) Synapses between M2/Cg terminals and PRF/GlyT2+ dendrites

A-D) Electron micrographs of M2/Cg terminals (DAB-Ni, dark, dense precipitate) establishing synapses on PRF/GlyT2+ dendrites (n=9, A), B), C), DAB, light precipitate) and spines (n=1, D) **E**) Boxplot of terminal sizes by type (terminals on GlyT2+ soma, on dendrite, and M2/Cg terminals) **F–H**) Histograms with KDE curves showing the size distribution of terminals contacting GlyT2+ somata (**F**), dendrites (**G**), and M2/Cg (**H**) terminals. *0.05<p; ** 0.01<p; *** p<0.001. Scale bar: 500 nm [32]

Chapter summary

- ➤ In the PRF, M2/Cg terminals varied from small to medium size, each containing 1-3 mitochondria. They formed asymmetrical synapses with active zones primarily targeting dendrites.
- Larger terminals containing multiple mitochondria were observed on GlyT2+ somata; however, they do not originate from the M2/Cg cortex.
- Monosynaptic contacts were proven between M2/Cg terminals and PRF/GlyT2+ neurons, with most postsynaptic structures consisting of mid-caliber dendrites and spines.

4.3. THALAMUS-PROJECTING PRF CELLS

So far, we have demonstrated that the M2/Cg cortical area directly innervates the dendrites of PRF/GlyT2+ neurons (see Figure 8). In turn, PRF/GlyT2+ cells project to their postsynaptic partners in the thalamus [20]. However, it remains to be directly shown whether the axons from cortical layer 5 can actually target the PRF/GlyT2+ neurons that innervate the thalamus and inhibit IL/Pf neurons.

To explore this issue, we injected a conditional retrograde AAVrg-hSyn-DIO-mCherry virus into the IL/Pf and anterograde AAV5-CAMKIIa-hChR2-eYFP into the M2/Cg regions of GlyT2-Cre mice (Figure 9). Subsequently, we investigated the GlyT2+ cells that were retrogradely labeled from the thalamus in the PRF, as well as the M2/Cg terminals that contacted them. We validated the cortical injection sites in M2/Cg (Figure 9A-B) and their thalamic projections in IL/Pf (Figure 9C-D). In the brainstem, we detected retrogradely labeled PRF/GlyT2+ neurons situated among the cortical fibers (Figure 9E-H). Using confocal microscopy, we confirmed that M2/Cg terminals formed potential contacts with 82% of all thalamus-projecting PRF/GlyT2+ dendrites (n=50, from 3 mice, Figure 9I-K). We calculated the mean number of close appositions in 50-μm-long dendritic segments, resulting in 2.4 ± 0.22 (Figure 9L).

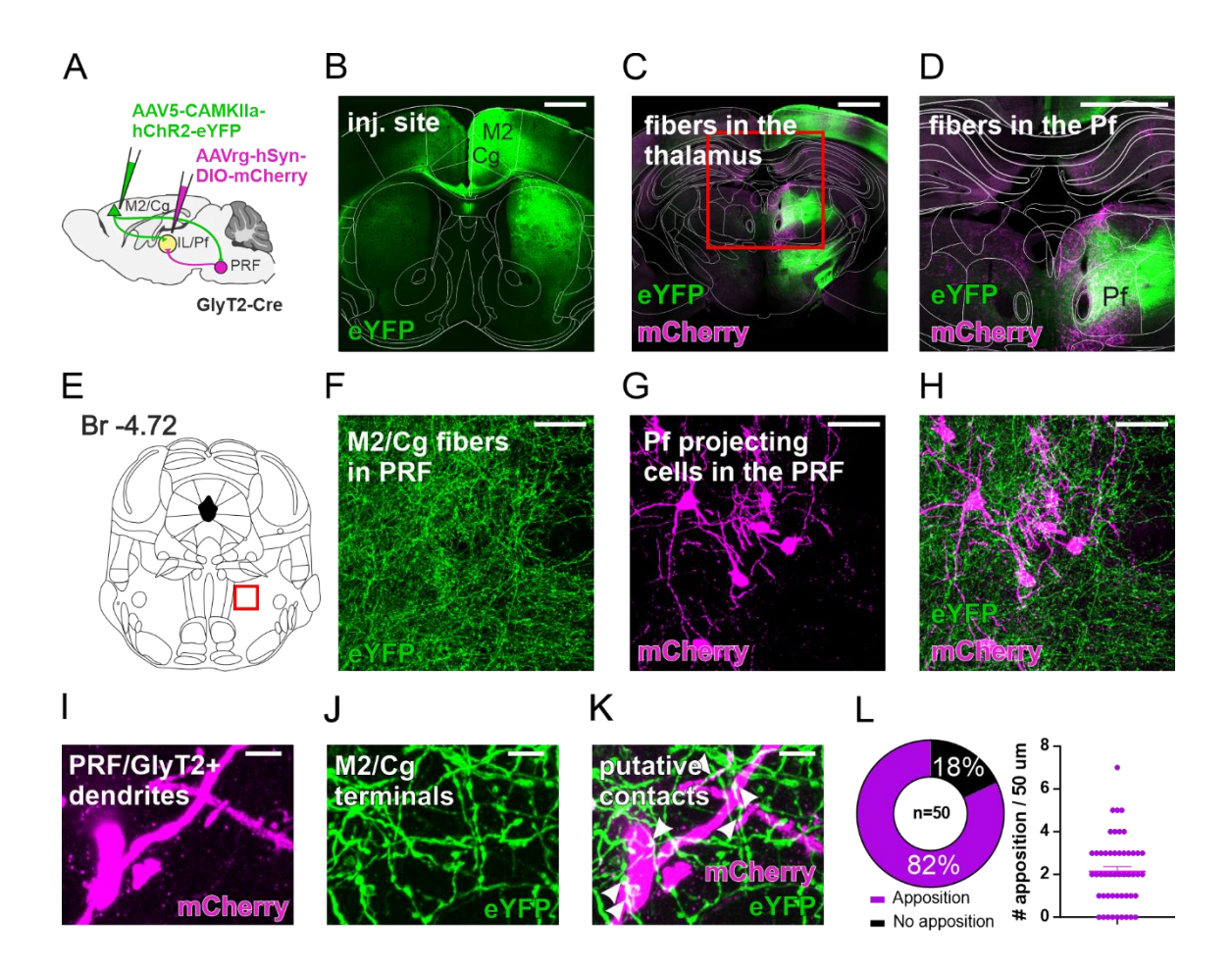


Figure 9) Cortical innervation of thalamus-projecting PRF/GlyT2+ cells

A) Scheme of the double conditional viral tracing to label cortical inputs to thalamus projecting PRF/GlyT2+ cells. B) Low-power confocal micrograph of the unilateral cortical injection site. C-D) Merged confocal image of the M2/Cg cortical fibers (green) and PRF/GlyT2+ fibers (magenta) in the thalamus. The red rectangle in C indicates the position of the D micrograph. E) Coronal, stereotactic image of the brainstem. The red rectangle indicates the position of the F-H micrographs. F-H) Confocal micrographs of the anterogradely labeled M2/Cg cortical fibers (green, F), retrogradely labeled thalamus-projecting PRF/GlyT2+ cells (magenta, G), and their merged image (H). I-K) High-power confocal microscopic image of the thalamus-projecting PRF/GlyT2+ dendrites (magenta, I) and M2/Cg fibers (green, J) and their putative contacts (K, arrowheads). L) Percentage of innervated thalamus-projecting PRF/GlyT2+ dendrite (left) and mean number of the close apposition per dendritic segment (right). Scale bars: B-D) 1 mm F-H) 50 μm I-K) 5 μm. [32]

Chapter summary

➤ Confocal microscopy demonstrated that M2/Cg terminals formed close appositions with the majority of thalamus-projecting PRF/GlyT2+ dendrites, supporting the existence of a functional pathway linking cortical layer 5 to thalamic inhibition via the PRF.

4.4. CO-INNERVATION OF PRF AND THE THALAMIC TARGETS OF PRF BY L5 NEURONS

L5 neurons that innervate the striatum have been shown to arborize in the thalamus. Since the basal ganglia also innervate the thalamus, and the thalamus projects back to the cortex, these three structures form multiple nested loops [7–9].

To investigate whether the same logic applies to individual L5 neurons targeting the PRF-specifically, whether L5 neurons simultaneously innervate both the PRF and the target region of PRF/GlyT2+ cells in the thalamus (the intralaminar and parafascicular nuclei, IL/Pf)- firstly we analyzed data from the Mouse Light Neuron Browser database [59] (https://www.janelia.org/open-science/mouselight-neuronbrowser). In the database, we found 23 M2/Cg L5 neurons with at least one axonal endpoint in the PRF (Figure 10A-C; Table 1). Seventy-four percent of these neurons (n=17) also projected to the IL/Pf. Ten of the M2/Cg L5 17 neurons (59%) co-innervating the PRF and IL/Pf exhibited multiple axonal endpoints (defined here as more than four endpoints) in both the PRF and IL/PF. Four of the 23 PRF projecting L5 neurons (17.4%) showed very dense axonal arbors in the PRF (more than ten axonal endpoints) (Figure 10C). Three of these L5 cells innervated the IL/Pf region, each with more than 10 axonal endpoints. The fourth cell formed 6 endpoints in IL/Pf. Confirming our anterograde tracing experiments, these neurons arborized more in the dorsomedial part of the PRF (Figure 10C). These data suggest that co-innervation of the PRF and IL/Pf by individual cortical L5 neurons is common.

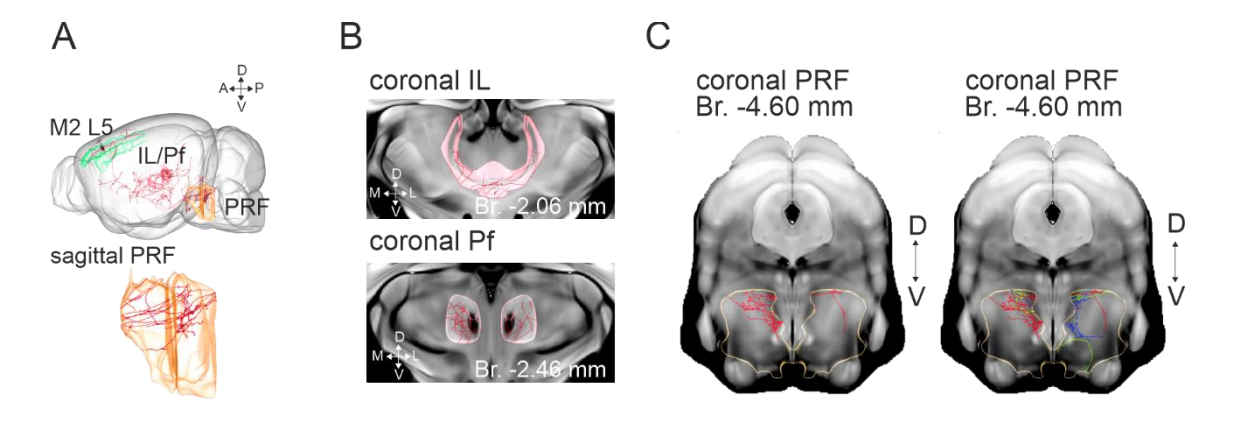


Figure 10) Co-innervation of PRF and IL/Pf by individual L5 neurons

A) Reconstruction of a representative M2 L5 (AA0245) neuron from the Mouse Light Neuron Browser database, which innervates both PRF and IL/Pf (top). Axon arbor of the representative M2 L5 neuron (AA0245) at the sagittal level in the PRF (bottom). **B)** Axon arbor of the representative M2 L5 neuron (AA0245) in the IL (top) and Pf (bottom) **C)** Axon arbor of the representative M2 L5 neuron (AA0245) (left in red) and of 4 L5 neurons in the PRF (right, red,

yellow, blue and green) that have 10 or more axonal end points in the PRF and also innervate IL/Pf with multiple endpoints. [32]

Sixteen of the 17 L5 neurons (94.12%) co-innervating the PRF and IL/Pf also had a collateral to the striatum, indicating that the cortico-PRF-thalamic message is also projected to the basal ganglia (Table 1).

Table 1) Co-innervation of PRF, IL/Pf, and the striatum by single L5 neurons

Co-innervation of PRF, IL/Pf, and the striatum by single M2/Cg L5 neurons					
			PRF		striatal
	Soma's		axonal	IL/Pf axonal	axonal
DOI	position	Entire name	endpoint	endpoint	endpoint
AA0179	MOs5	Secondary motor area layer 5	1	2	+
		Anterior cingulate area			
AA0845	ACAv5	ventral part layer 5	1	0	-
AA0115	MOs5	Secondary motor area layer 5	2	4	+
		Anterior cingulate area dorsal			
AA0764	ACAd5	part layer 5	2	3	+
		Anterior cingulate area			
AA0796	ACAv5	ventral part layer 5	3	0	-
AA0882	MOs5	Secondary motor area layer 5	3	0	-
AA1544	MOs5	Secondary motor area layer 5	3	4	-
AA0181	MOs5	Secondary motor area layer 5	4	44	+
AA0415	MOs5	Secondary motor area layer 5	4	2	+
AA0576	MOs5	Secondary motor area layer 5	4	1	+
AA0792	MOs5	Secondary motor area layer 5	4	20	+
AA0182	MOs5	Secondary motor area layer 5	5	14	+
AA0250	MOs5	Secondary motor area layer 5	6	1	+
AA0780	MOs5	Secondary motor area layer 5	6	7	+
AA1538	MOs5	Secondary motor area layer 5	6	0	-
AA0114	MOs5	Secondary motor area layer 5	7	5	+
AA0791	MOs5	Secondary motor area layer 5	8	6	+
AA0180	MOs5	Secondary motor area layer 5	9	0	-
AA1541	MOs5	Secondary motor area layer 5	12	0	-
AA0772	MOs5	Secondary motor area layer 5	19	31	+
AA0788	MOs5	Secondary motor area layer 5	19	6	+
AA0261	MOs5	Secondary motor area layer 5	37	36	+
AA0245	MOs5	Secondary motor area layer 5	39	34	+

Neuron database based on Janelia Mouse Browser. DOI: Janelia ID for neurons. Soma's position name was determined by Janelia's nomenclature PRF and IL/Pf axonal endpoint, which means how many afferents the PRF has from M2/Cg. In the striatal axonal endpoint column, the \pm -indicates whether there was M2/Cg's afferent. [32]

The Mouse Light Neuron Browser data does not allow us to determine whether the cortico-PRF-thalamic neurons target PRF/GlyT2+ cells or other cell types in the PRF. To demonstrate that thalamic-projecting cortical cells can innervate PRF/GlyT2+ cells, we employed two experimental designs (Figures 11 and 12).

In the first configuration, we injected AAVrg-EF1a-DIO-FlpO into the IL/Pf and AAV2/1-EF1a-fDIO-mCherry into the M2 region of RPB4-Cre//GlyT2-eGFP mice (Figure 11A). In this scenario, Flp is Cre-dependent, travels retrogradely from the

thalamus to the cortex, and is expressed in RBP4+ L5 neurons (Figures 11B-C). The second virus is FLP-dependent and travels anterogradely from these L5 neurons projecting to the IL/Pf (Figures 11D-K). We observed retrogradely labeled deep layer M2/Cg pyramidal cells (Figure 11C) and a dense axonal arbor in the dorsolateral Pf/IL, confirming the injection sites and thalamic projections (Figure 11D).

Dense cortical innervation was also observed in the PRF in every case (n=4 animals), specifically in the same PRF/GlyT2+ area (Figures 11I-L) identified following our initial M2/Cg AAV5-DIO-ChR2-mCherry injections (as indicated in Figure 2). The cortical projection was primarily ipsilateral in the PRF.

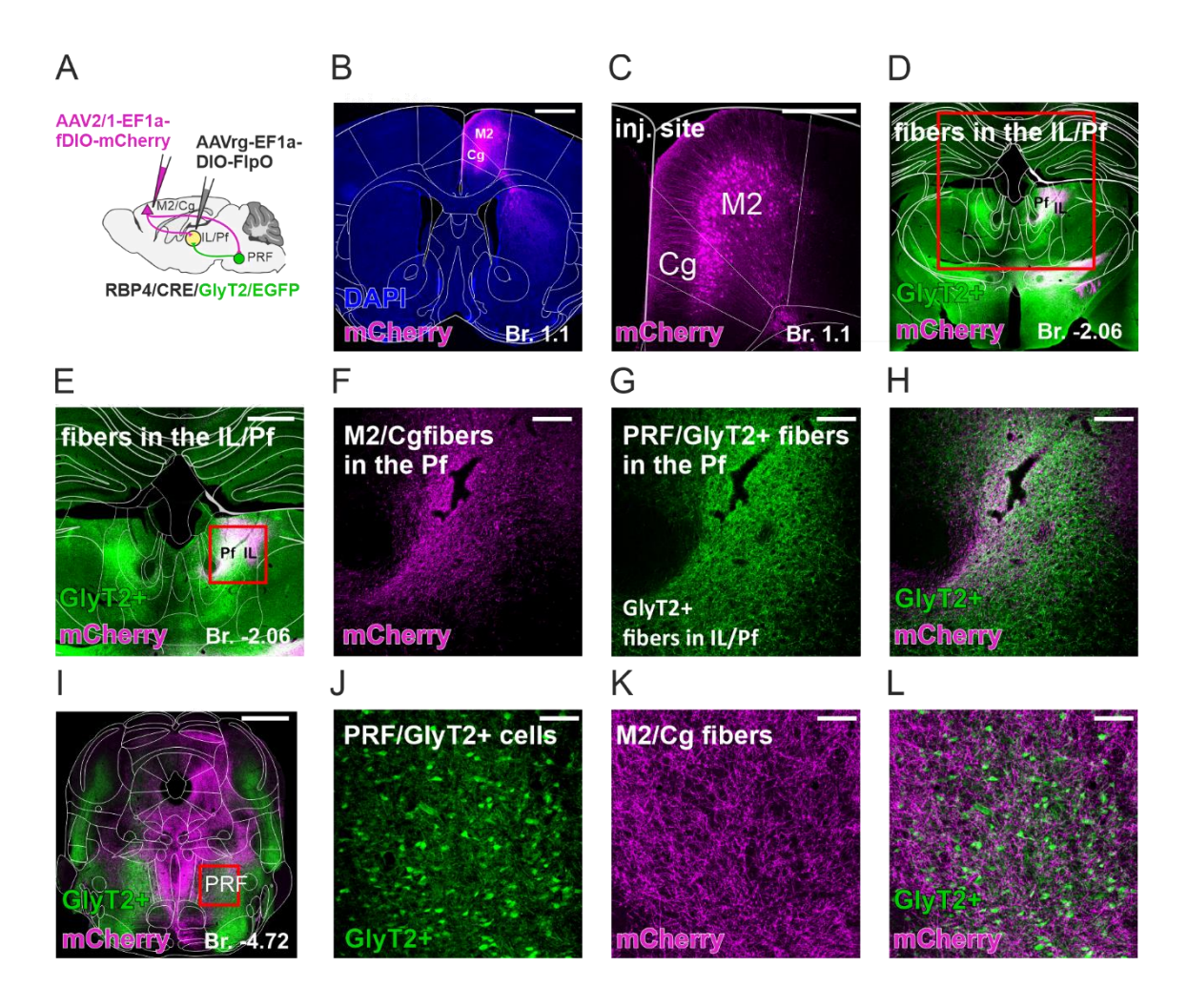


Figure 11) Co-innervation of the PRF and thalamus by M2/Cg L5 neurons – first design

A) Scheme of the viral tracing to label PRF collaterals of thalamus-projecting M2/Cg cells. **B**) Low-power confocal micrograph of the cortical M2/Cg injection site. **C**) High-power confocal fluorescent image of the thalamus-projecting M2 L5 neurons. **D-E**) Merged confocal image of the labeled thalamus-projecting M2/Cg cortical fibers (magenta) and PRF/GlyT2+ fibers (green) in the thalamus. **F-H**) Confocal image of the labeled thalamus-projecting M2/Cg cortical fibers (magenta, **F**), of the PRF/GlyT2+ fibers (green, **G**) and their merged image (**H**). **I**) Merged, low power confocal image of the labeled thalamus-projecting M2/Cg cortical fibers (magenta) and PRF/GlyT2+ fibers (green) in the brainstem. **J-L**) Confocal micrographs of the PRF/GlyT2+ cells (green, **J**), anterogradely labeled thalamus-projecting M2/Cg cortical fibers (magenta, **K**), and their merged image (**L**). Scale bars: B) 1 mm, C) 500 μ m E) 1 mm F-H)100 μ m I) 1 mm J-L) 100 μ m [32]

In the second approach, we injected a Cre-expressing retrograde virus (AAVrg-EF1a-Cre) into the IL/Pf and the AAV5-EF1a-DIO-hChR2-mCherry virus into the M2 of GlyT2-EGFP mice (see more details in the Methods; Figure 12A). Similar to the first design, we observed retrogradely labeled cortical cells (Figures 12B-C) and dense

innervation in the thalamus (Figures 12D-H). The PRF was also similarly innervated ipsilaterally (Figure 12I-L).

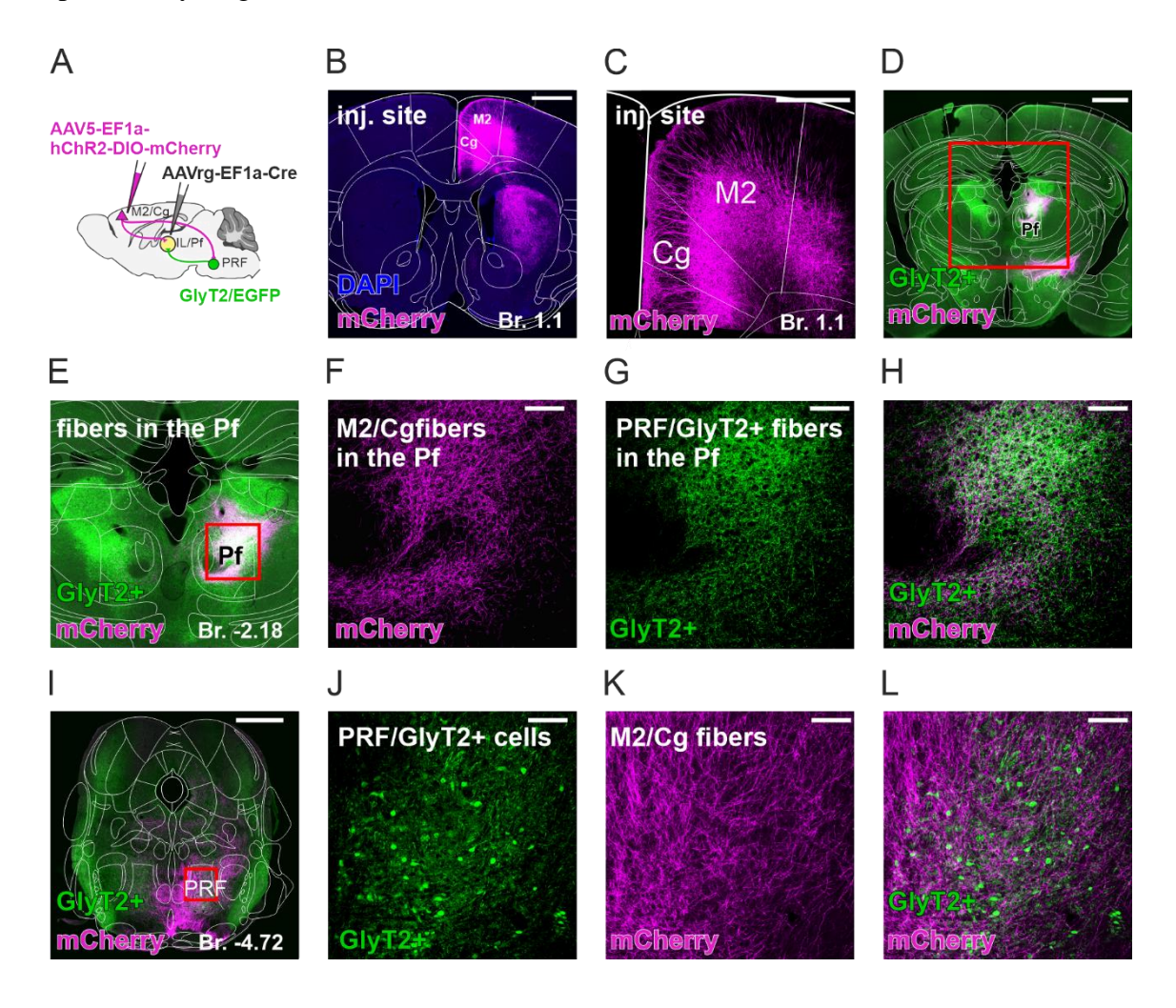


Figure 12) Co-innervation of the PRF and thalamus by M2/Cg L5 neurons – second design

A) Scheme of the second experimental design, double viral injection in GlyT2/eGFP mice **B-C**) Fluorescent micrograph of the cortical injection site, low power (**B**) and confocal image of the cortical neurons (**C**). **D-E**) Merged fluorescent image of the labeled thalamus-projecting M2/Cg cortical fibers (magenta) and PRF/GlyT2+ fibers (green) in the thalamus at lower (**D**) and higher (**E**) magnification. The red rectangle on **D** indicates the area in **E** and the red rectangle on E indicates the **F-H** position. **F-H**) Confocal image of the labeled thalamus-projecting M2/Cg cortical fibers (magenta, **F**), of the PRF/GlyT2+ fibers (green, **G**) and their merged image (**H**) in the thalamus. **I**) Composite fluorescent image of the labeled thalamus-projecting M2/Cg cortical fibers (magenta) and PRF/GlyT2+ fibers (green) in the brainstem **J-L**) Confocal micrographs of the PRF/GlyT2+ cells (green, **J**), anterogradely labeled thalamus-projecting M2/Cg cortical fibers (magenta, **K**), and their merged image (**L**) Scale bars: B) 1 mm, C) 500 μm, D-E) 1 mm, F-H) 100 μm, I) 1 mm J-L) 100 μm [32]

Using high-resolution confocal microscopy, we identified close appositions between the axons of IL/Pf projecting cortical neurons and the dendrites of PRF/GlyT2+ cells (Figure 13A-D).

In the first experimental configuration, 72.5% of PRF/GlyT2+ dendrites (n=40) were contacted by the axon terminals of thalamic projecting M2/Cg axons, compared to 65% in the second experiment (n=40). The average number of close appositions per dendrite was 2.125 ± 0.308 in the first case and 1.45 ± 1.339 in the second. The pooled data indicate that 69% of the PRF/GlyT2+ dendritic segments (n=80) were juxtaposed to M2/Cg boutons, with an average of 1.45 ± 1.339 putative contacts per 50 μ m segment (Figure 13D). Together, these data demonstrate that thalamus-projecting M2/Cg pyramidal cells can also innervate PRF/GlyT2+ cells.

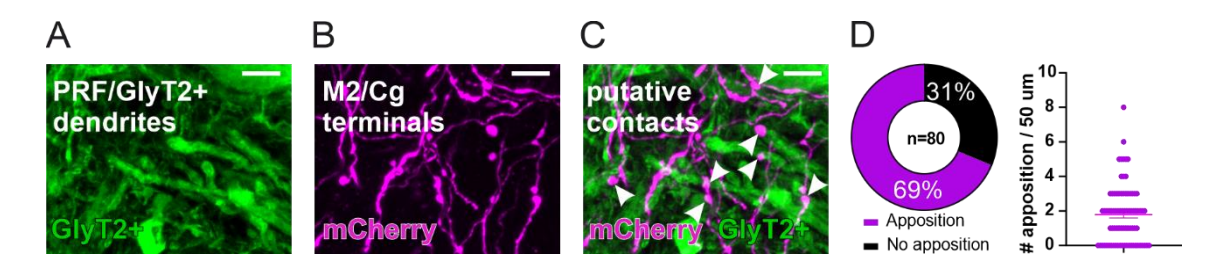


Figure 13) Thalamus-projecting M2/Cg axon arbors in the PRF and the thalamus

A-C) High power confocal microscopic image of close apposition between the PRF/GlyT2+ dendrites (green, **A**) and thalamus-projecting M2/Cg fibers (magenta, **B**). Arrows, putative contacts in (**C**). **D**) Percentage of innervated PRF/GlyT2+ dendrite (left) and the mean number of the close apposition per dendritic segment (right). [32]

This data shows that the same layer 5 cell can innervate PRF/GlyT2+ cells and IL/PF. Together with the data where we identified cortical inputs on thalamic-projecting PRF/GlyT2+ cells, we demonstrated that in this system, the cortex, PRF/GlyT2+ cells, and thalamus can form multiple nested loops.

Chapter summary

- ➤ M2/Cg pyramidal neurons can simultaneously target PRF and IL/Pf, with further collaterals reaching the striatum.
- Thalamus-projecting M2/Cg cortical neurons innervate PRF/GlyT2+ cells

4.5. ACTIVATION OF PRF/GLYT2+ NEURONS PROMOTES ROTATIONAL MOVEMENTS

Next, we aimed to examine the behavioral effects of activating thalamus-projecting PRF/GlyT2+ cells, a key node in the cortex-PRF-thalamus connection communication. To address this, we injected AAV5-DIO-ChR2-eYFP into the PRF of GlyT2-Cre animals and implanted fiber optics into the thalamus (IL/Pf) (n=7 stimulus sites, n=2 animals). We then photoactivated PRF/GlyT2+ fibers unilaterally and bilaterally at various laser intensities (Figure 14A) in IL/Pf. Bilateral stimulation (n=20 stimulation) or unilateral stimulation with higher (15 mW) laser intensities (n=24 stim) resulted in behavior arrest, confirming earlier data [20]. Unilateral stimulation of PRF/GlyT2+ axons in the IL/Pf at lower laser intensity (1, 5, and 10 mW), however, always induced rotation in the contralateral direction (Figure 14B).

The mean rotation angle was measured before, during, and after the stimulus periods, focusing on contralateral rotations. The average percentage of a full 360° rotation per second was calculated (Figure 14B), and statistical analysis revealed a significant difference ($\chi^2 = 10.6$, p = 0.005, Friedman test, followed by Durbin-Conover post-hoc comparisons). Specifically, there was a marked increase in rotational movements before stimulation compared to during stimulation (p < 0.001) and between stimulation and after the stimulus (p < 0.001) (Figure 14B). The positions of the optic fibers were identified post hoc (Figure 14C). These results demonstrate that the activation of thalamic-projecting PRF/GlyT2+ cells through their axons in the IL/Pf consistently induces contralateral rotation.

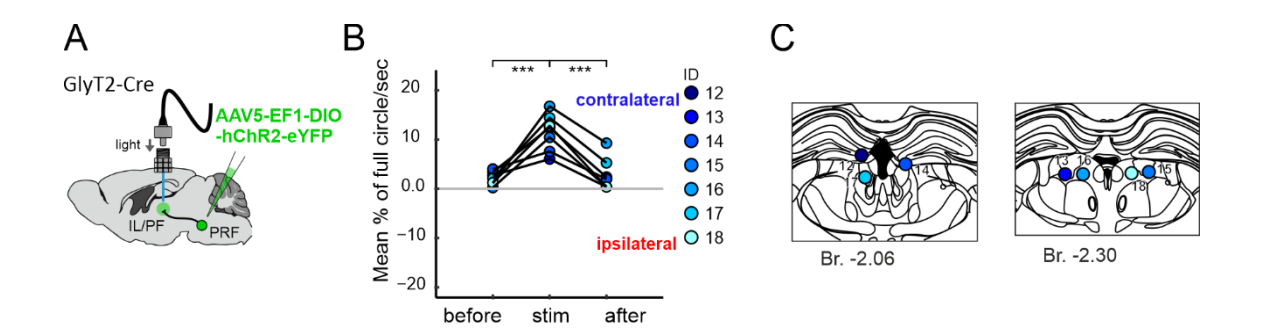


Figure 14) Photostimulation of PRF/GlyT2+ fibers in the thalamus

A) Experimental design of the photoactivation of thalamus-projecting PRF/GlyT2+ cells via their fibers in the thalamus (n=7 fiber optic fibers). **B)** Contralateral rotations (n=7 fiber optics) displayed as mean rotation angle before, during, and after the stimulus periods following PRF/GlyT2+ fiber stimulation in Pf. **C)** Schematic view of post hoc identified 7 optic fiber positions for experimental animals in Pf. [32]

However, not all PRF/GlyT2+ cells may project to the thalamus. To identify whether the behavioral effect of activating thalamus-projecting PRF/GlyT2+ cells differs from that of the overall PRF/GlyT2+ population, we injected AAV5-DIO-ChR2-eYFP into the PRF of GlyT2-Cre animals and implanted fiber optics into the PRF. We then photoactivated PRF/GlyT2+ neurons unilaterally via their somata (Figure 15A) at various laser intensities (1, 5, 10, 15 mW; 5 ms pulse at 40 Hz for 10 sec, n=7 animals).

Firstly, we analyzed the rotational movements during the stimulation of PRF/GlyT2+ somata in the animals (10 seconds of stimulation; see Figure 15B)). Across the entire sample (n=7 optic fibers), optogenetic activation resulted in a significant increase in rotational behavior at all stimulation intensities (Figure 15C; Friedman tests: 1 mW: χ^2 =6, p=0.050; 5 mW: χ^2 =8.33, p=0.016; 10 mW: χ^2 =10.3, p=0.006; 15 mW: χ^2 =12.3, p=0.002). Post hoc Durbin-Conover analysis indicated that rotational movement significantly increased from baseline to stimulation (1 mW: p=0.073; 5 mW: p=0.038; 10 mW: p<0.001; 15 mW: p<0.001) and then significantly decreased from stimulation to the post-stimulation period (1 mW: p=0.012; 5 mW: p<0.001; 10 mW: p=0.014; 15 mW: p=0.004). However, similar to the previous analysis, no significant dose-response relationship was observed with increasing light intensity (Friedman test: χ^2 =7, p=0.072; see Figure 15D).

Interestingly, somatic stimulation of PRF/GlyT2+ neurons induced contralateral rotational movements in 4 out of 7 animals, similar to the effects observed with thalamic

stimulation of PRF/GlyT2+ fibers. The remaining 3 animals exhibited ipsilateral rotation (Figure 15E). We found no significant differences in rotational angles between the ipsi and contralateral turning animals (ipsi vs. contralateral stimulation for all intensity: U=2, p=0.229). Post hoc histological identification of optic fiber positions within the PRF revealed no discernible anteroposterior, dorsoventral, or mediolateral differences between the animals that displayed ipsi or contralateral rotational movements (Figure 15F-H).

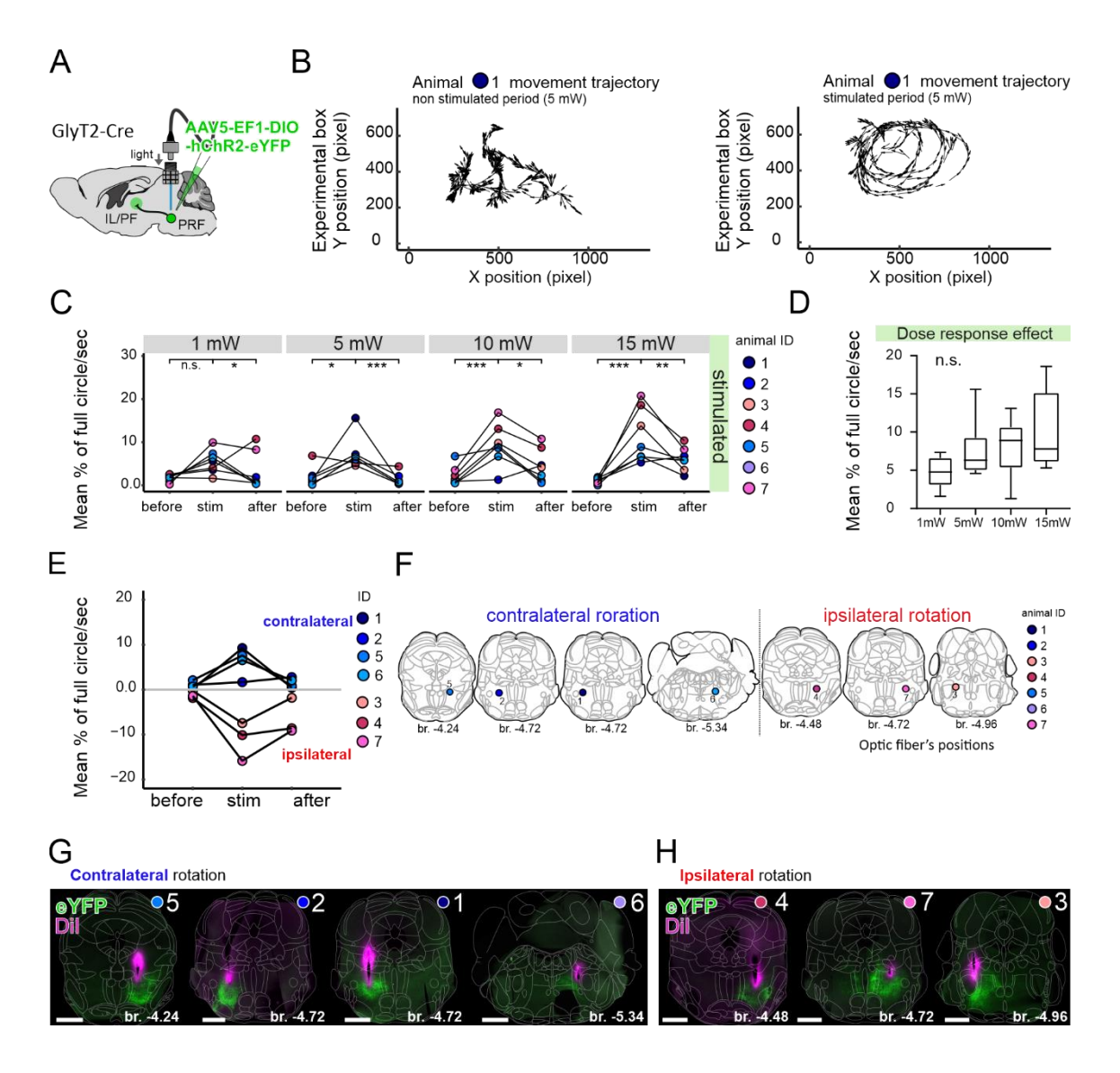


Figure 15) Behavioral effects of unilateral optogenetic activation of PRF/GlyT2⁺ neurons

A) Schematic illustration of the experimental setup **B**) Movement trajectory in one representative mouse displaying contralateral turning (mouse ID: 1). Non-stimulated period (left), stimulated period (right) at 5 mW in the PRF. **C**) Comparison of the absolute values of the mean rotation angle before, during, and after the PRF stimulus periods in the 7 experimental mice **D**) Lack of significant dose-response effect on rotation. **E**) Contralateral (n=4 animals, blueish shades) and ipsilateral (n=3 animals, reddish shades) rotations following PRF/GlyT2 somatic stimulations. The color code of the animals is the same as in **C**. **F**) Schematic view of post hoc identified optic fiber position (n=7) in PRF for the 7 experimental mice. Right: fiber optic positions inducing contralateral rotation; left: fiber optic positions inducing ipsilateral rotation. Same notation as in **E**. **G-H**) Fluorescent micrographs of the implanted optic fibers in mice responding with contralateral (**G**) and ipsilateral (**H**) rotation to unilateral activation of PRF/GlyT2+ somata. * 0.05<p; ** 0.01<p; *** p<0.001; n.s. - no significant difference. cale bars: G-H) 1 mm [32]

Since the effect of PRF/GlyT2+ soma activation on movement initiation and maintenance has not been characterized, we measured the speed during the initial second of the PRF/GlyT2+ stimulation and the following 9 seconds (Figure 16A).

We observed significant changes in speed at 1 mW (χ^2 =7.14, p=0.028) and 10 mW (χ^2 =9, p=0.050), while no significant effects were found at 5 mW (χ^2 =4.33, n.s.) or 15 mW (χ^2 =6, n.s.) (Figure 16A). We performed a Durbin-Conover post hoc analysis for the 1 mW and 10 mW conditions to identify where these differences occurred. In both cases, movement significantly increased during the first second of stimulation compared to baseline (1 mW: p=0.004; 10 mW: p=0.012), and this elevated activity persisted throughout the remaining 9 seconds. However, no further significant differences were found between the first second and the last 9 seconds, or between baseline and the last 9 seconds. Additionally, we did not find a significant dose-response effect, as higher laser intensities did not produce proportionally greater movement during the first second (Friedman test: χ^2 =4.2, n.s.; see Figure 16B).

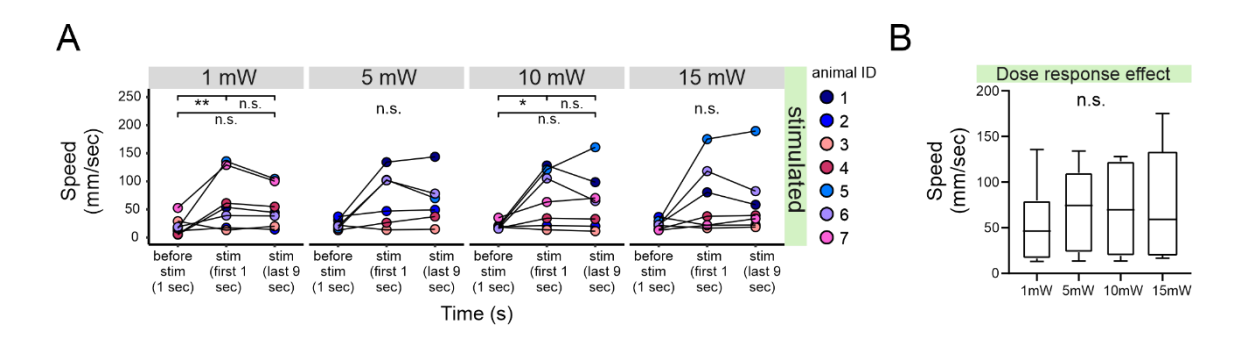


Figure 16) Speed during PRF/GlyT2+ soma photoactivation

A) Comparison of the speed (mm/sec) before the stimulus, in the first 1 sec and the subsequent 9 sec during the stimulus in the experimental animals (n=7). Numbers indicate individual animals. **B)** Lack of dose-response effect at 1, 5, 10, and 15 mW laser power in experimental mice on movement initiation. [32]

In the control group, we injected the AAV5.EF1a.DIO.eYFP virus into the PRF to examine the initiation and rotation effect (n = 4 animals, Figure 17A-C). The speed showed no significant differences (Figure 17, ; Friedman tests for speed 1 mW: $\chi^2=1.5$, n.s., 5 mW: $\chi^2=0.5$, n.s., 10 mW: $\chi^2=0$, n.s., and 15 mW: $\chi^2=0.5$, n.s.) (Figure 17D). Furthermore, no dose-response effect for speed was found (Friedman test for the first second: $\chi^2=6.9$, n.s.) (Figure 17E). Similarly, for rotation, no significant differences were observed at any intensity (Figure 17F, Friedman tests for rotation: 1 mW: $\chi^2=0$, n.s., 5

mW: χ^2 =1.5, n.s., 10 mW: χ^2 =1.5, n.s., and 15 mW: χ^2 =4.5, n.s.). The dose-response analysis for rotation also showed no significant results (Figure 17G, Friedman test χ^2 =1.2, n.s.).

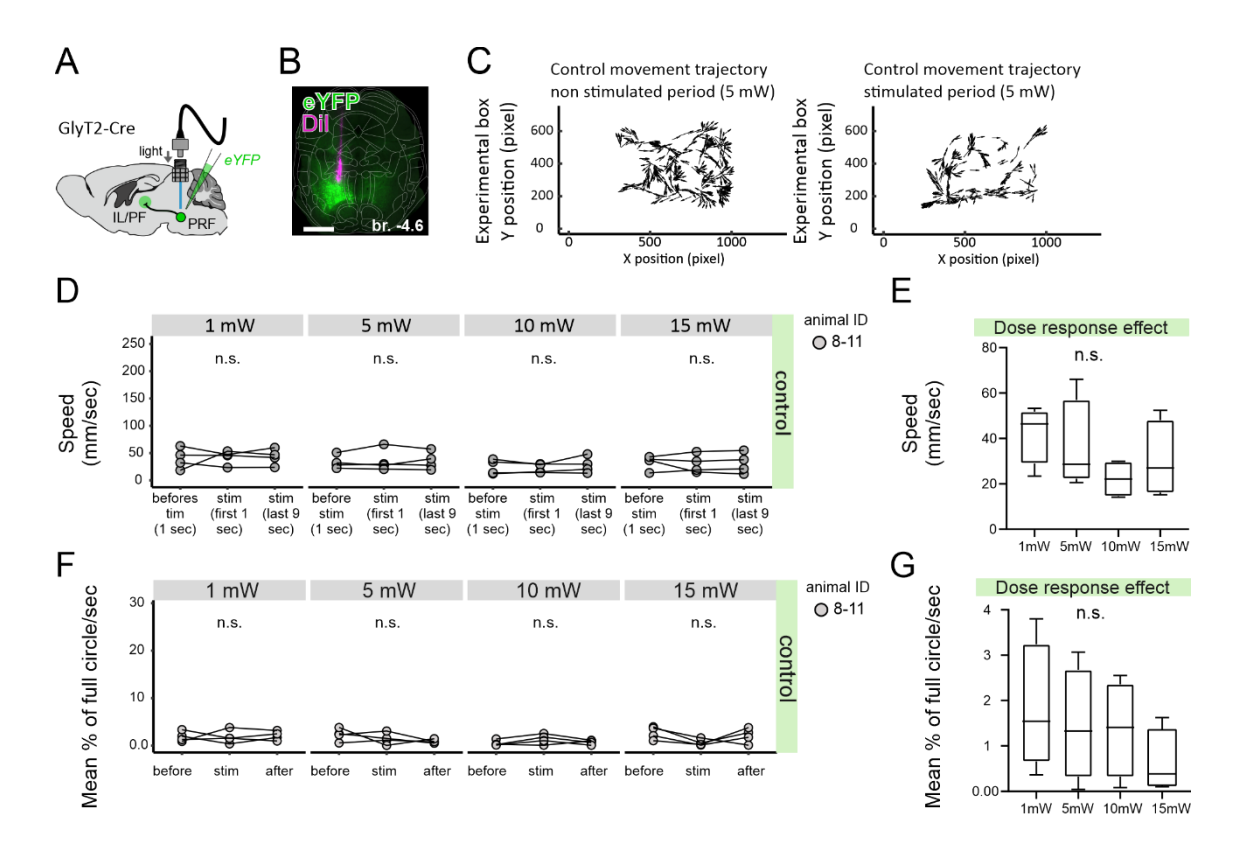


Figure 17) Behavioral effects of photoactivating PRF/GlyT2+ somata in control (EYFP) conditions

A) Experimental design of the control behavioral experiments in GlyT2-Cre mouse. **B)** Fluorescent micrographs of the implanted optic fiber in representative control mice. **C)** Movement trajectory in one representative control mouse during the non-stimulated period (left) and the stimulated period (right) at 5 mW. **D)** Comparison of the speed (mm/sec) before the stimulus, in the first 1 sec and the subsequent 9 sec during the stimulus in control animals. **E)** Lack of doseresponse effect at 1, 5, 10, and 15 mW laser power in control mice on movement initiation. **F)** Control animals' mean rotation angle before, during, and after stim periods. **G)** Lack of doseresponse effect at 1, 5, 10, and 15 mW laser power in control mice on rotation. *0.05<p; *** 0.01<p; *** p<0.001; n.s. - no significant difference. Scale bar B) 1 mm [32]

Next, we conducted loss-of-function experiments by injecting AAV5-DIO-eNpHR 3.0-eYFP into the PRF (n=4 animals) and implanting optic fibers in the PRF (n=8 optic fibers; Figure 18A). Similar to the gain-of-function experiments (Figures 15 and 16), we found that inhibiting PRF/GlyT2+ somata unilaterally could result in both contraversive and ipsiversive rotations (Figure 18B). However, no significant differences in rotational angles were found for the whole group (Figure 18C; Friedman test: 1 mW: χ^2 =3, n.s.; 5

mW: χ^2 =0.25, n.s.; 10 mW: χ^2 =3.25, n.s.; 15 mW: χ^2 =1, n.s.). A dose-response analysis for rotational behavior also showed no significant effect (Figure 18D; Friedman test: χ^2 =4.2, n.s.). Speed was significantly affected only at 15 mW (Figure 18E, Friedman test: 1mW χ^2 =2.25, n.s.; 5mW χ^2 =5.25, n.s.; 10mW χ^2 =1.75, n.s.; 15mW χ^2 =7.75, p=0.021). The Durbin-Conover post hoc analysis for 15 mW showed a significant increase during the first second of stimulation (before vs. first second: p = 0.039), indicating movement initiation. However, no significant differences were found between the first second and the last 9 seconds, or between baseline and the last 9 seconds. No significant dose-response relationship was found for movement initiation (Figure 18F; Friedman test for first sec: χ^2 =3.45, n.s.).

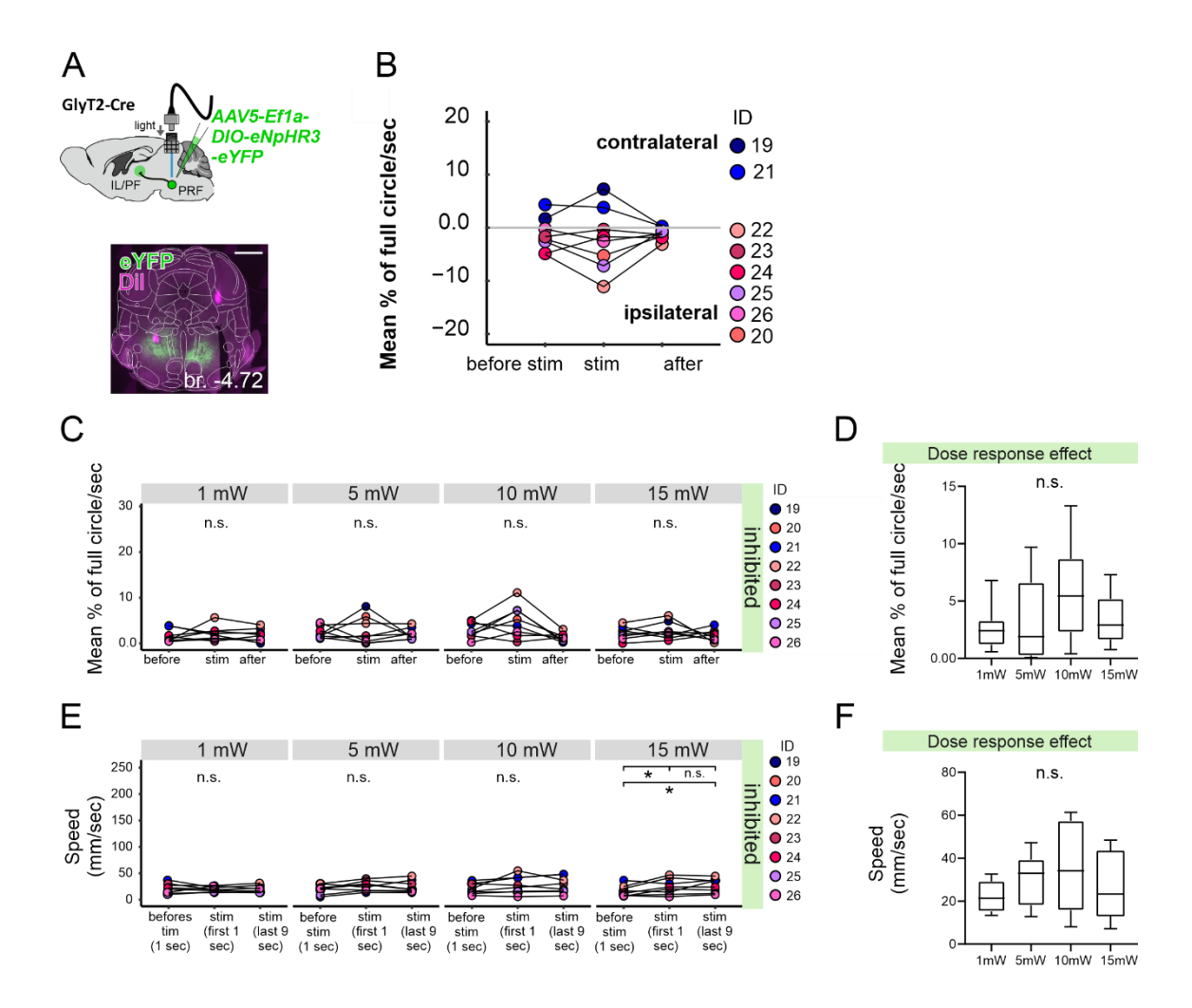


Figure 18) Behavioral effects of photoinhibiting PRF/GlyT2+ somata

A) Top: Experimental design of the photoinhibition behavioral experiments in GlyT2-Cre mouse Bottom: Fluorescent microscopic post hoc identification of implanted optic fiber and virus injection site (green) in one representative photoinhibited mouse. The appropriate optic fiber position was on the left side of the PRF labeled with DiI (magenta). B) Separation of the absolute rotational values into contralateral and ipsilateral rotations. The data is displayed as the mean rotation angle before, during, and after the stimulus periods following PRF/GlyT2+ soma inhibition at all intensities. C) Mean rotation angle of photoinhibited animals before, during, and after stim periods D) Lack of significant dose-response effect on rotation at 1, 5, 10, and 15 mW in control mice . E) Comparison of the speed (mm/sec) before the stimulus, in the first 1 sec and the subsequent 9 sec during the stimulus in photoinhibited animals. F) Lack of significant dose-response effect on movement initiation at 1, 5, 10, and 15 mW in control mice. * 0.05<p; *** 0.01<p; *** p<0.001; n.s. - no significant difference. Scale bar: A) 1 mm [32]

These findings show that activating PRF/GlyT2+ neurons can result in rotational movements. When thalamic projecting PRF/GlyT2+ cells are activated via their axons, contralateral turning occurs, whereas activating the entire PRF/GlyT2+ cell population can trigger both ipsilateral and contralateral turning.

Chapter summary

- ➤ Photostimulation of the inhibitory GlyT2+ fibers in the II/Pf induced contralateral rotations only
- ➤ Photostimulation of the PRF/GlyT2+ somata induced movement initiation at 1 mW and 10 mW, but no effects at 5 mW or 15 mW.
- ➤ Photostimulation of the PRF/GlyT2+ somata triggered significant rotational movements at all intensities. Both contraversive and ipsiversive rotations were observed in different animals.
- ➤ Inhibition of PRF/GlyT2+ somata caused both contraversive and ipsiversive rotations with no significant change. Significant movement initiation was observed only at 15 mW.
- No significant dose-response relationships were observed for movement or rotation at any intensity, indicating that increasing the intensity had no additional effect.

4.6. DISTINCT PROJECTION PATTERNS OF THALAMUS PROJECTING PRF/GLYT2+ CELLS

Next, we examined whether distinct projection patterns could explain the differences in turning behavior between PRF/GlyT2+ neurons that innervate the thalamus and the entire PRF/GlyT2+ population (Figure 19). Our primary focus was on the gigantocellular nucleus in the medulla (Gi), which has recently been shown to be responsible for the motor commands of turning movements. We compared ipsilateral and contralateral projections [2,17,19].

We investigated the output of thalamus-projecting PRF/GlyT2+ cells by injecting a retrograde Cre-dependent FlpO-containing virus (AAVrg-EF1a-DIO-FlpO) into the IL/Pf thalamus and AAV2/1-EF1a-fDIO-mCherry (n=3) into the PRF of GlyT2-Cre mice (Figure 19A1). This approach selectively labels the axon arbor of thalamus-projecting PRF/GlyT2+ cells (Figure 19A2-3). To label the axons from the entire PRF/GlyT2+ population, we injected AAV5-Ef1-DIO-eYFP into the PRF of GlyT2-Cre animals (n=4; Figure 19B1).

We identified a stark difference in the innervation pattern of the Gi between the two approaches. Thalamus-projecting PRF/GlyT2+ cells provided significantly more axons to the ipsilateral Gi (Figure 19A4-5; paired t-test, t(2)=22.07, p=0.002, n=3 mice), whereas labeling the entire PRF/GlyT2+ population (Figuree 19B2-3 resulted in ipsi- and contralateral axons in the Gi of similar density (Figure 19B4-5; paired t-test, t(3)=1.462, p=0.24, n=4) mice).

Recent data have indicated that excitatory, vGlut2-positive PRF cells project to the contralateral Gi and are responsible for contraversive turning [17]. Our data here, however, demonstrate that a subpopulation of inhibitory PRF cells mainly projects ipsilaterally but still induces contraversive turning. To directly illustrate the difference between the projection patterns of the excitatory and inhibitory PRF populations, we utilized the fact that glycinergic cells are GABAergic as well (2,14) and used double transgenic vGAT-Flp//vGlut2-Cre mice to label both the excitatory and inhibitory projections in the same animals (Figure 19C-E). We co-injected AAVDj-EF1a-fDIO-eYFP (cyan) and AAV5-hSyn-DIO-mCherry (magenta) unilaterally into the PRF (Figure 19C1) and examined the Gi (n=3). We could confirm that vGlut2+ neurons provide significantly more axons to the contralateral Gi side as described before (Figure 19C;

(paired t- test, $t_{(2)}$ =19.04, p=0.0027, n=3 mice), while vGAT+ neurons project bilaterally (Figure 19D), with a significantly higher fiber density on the ipsilateral side (paired t-test, t(2)=5.61, p=0.0303, n=3 mice).

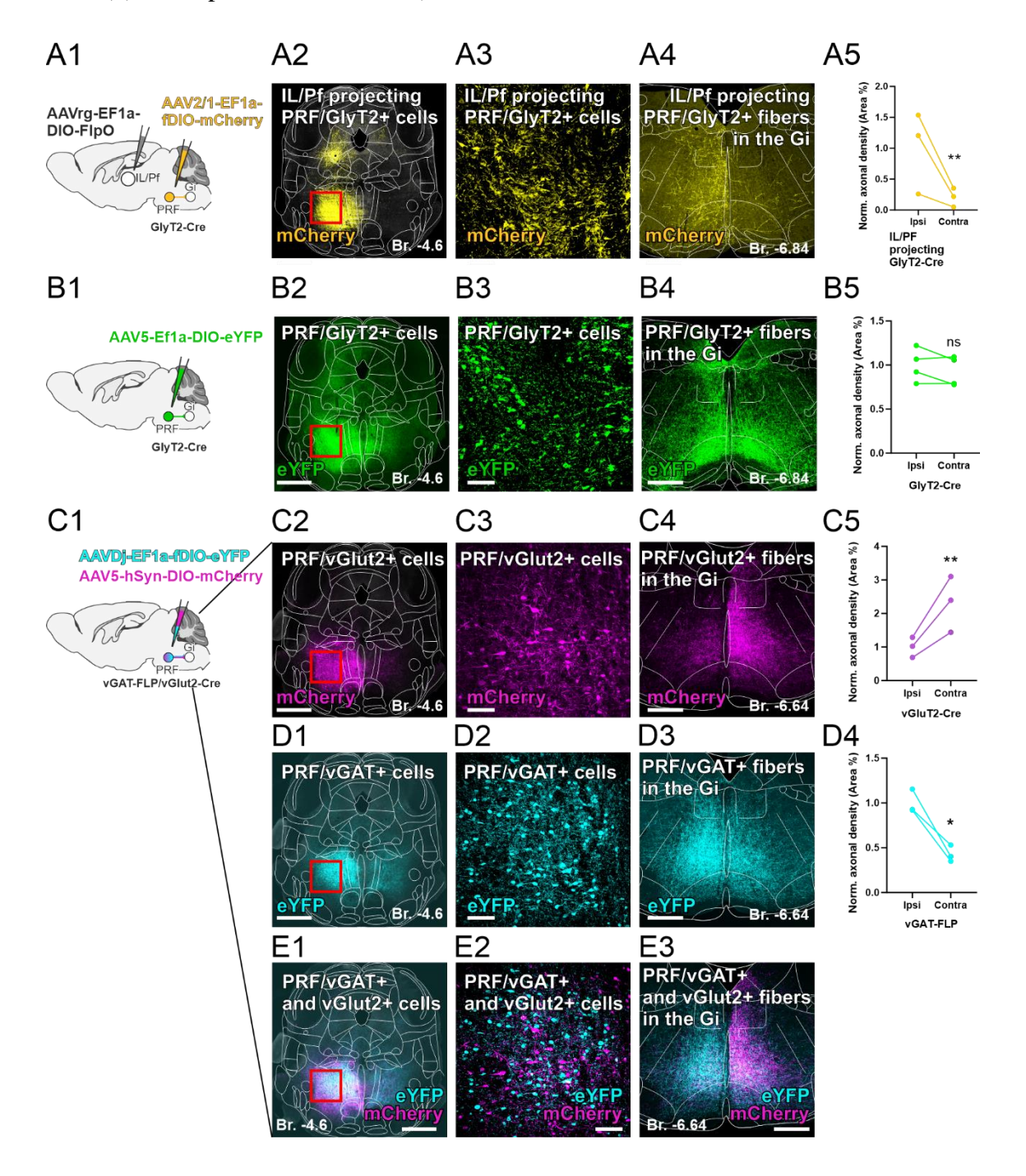


Figure 19) Selective ipsilateral innervation of the gigantocellular nucleus by thalamus projecting PRF/GlyT2+ cells

A1) Experimental design to label thalamus-projecting PRF/GlyT2 cells+ and their axons (n=3 mice). **A2-3**) Fluorescent micrograph about virus injection site in the PRF. The red rectangle on A2 indicates the position of the A3 micrograph. **A4**) Ipsilateral projection of the thalamus-

projecting PRF/GlyT2+ cells in the Gi (yellow) A5) Quantification of ipsilateral and contralateral axonal projections of the thalamus-projecting PRF/GlyT2+ cells in the Gi in GlyT2-Cre Mice B1) Experimental design to label all PRF/GlyT2 cells+ PRF (n=4 mice). B2-3) Fluorescent micrograph about virus injection site in PRF. The red rectangle on B2 indicates the position of the B3 micrograph. **B4**) Bilateral projection of the PRF/GlyT2+ cells in the Gi (green). **B5**) Quantification of the ipsilateral vs. contralateral axonal projections from PRF/GlyT2+ cells within the Gi Region in GlyT2-Cre mice . C1) Scheme of mixed viral injection into PRF in vGAT-Flp/vGlut2-Cre (n=3 mice). C2-3) Fluorescent micrograph about virus injection site in PRF. The red rectangle on C2 indicates the position of the C3 micrograph. C4) Bilateral projection with contralateral dominance of PRF/vGlut2+ cells in the Gi (magenta). C5) Quantification of ipsilateral and contralateral axonal projections from PRF/vGluT2+ cells within the Gi Region in vGluT2-Cre/vGAT-FLP mice **D1-2**) Fluorescent micrograph about virus injection site in PRF. The red rectangle on D1 indicates the position of the D2 micrograph **D3**) Bilateral projection with ipsilateral dominance pf PRF/vGAT cells in the Gi (cyan) **D4**) Quantification of ipsilateral and contralateral axonal projections from PRF/vGAT2+ cells within the Gi Region in vGluT2-Cre/vGAT-FLP mice . E1-2) Fluorescent micrograph about virus injection site in PRF. The red rectangle on E1 indicates the position of the E2 micrograph. E3) Merged image of PRF/vGAT (cyan) and PRF/vGlut2+ (magenta) fibers in the Gi. * 0.05<p; ** 0.01<p; *** p<0.001; n.s. - no significant difference. Scale bars: A2/B2/C2/D1/E1) 500 µm; A3/B3/C3/D2/E2) 100 µm A4/B4/C4/D3/E3) 500 µm [32]

As previously described, the thalamic projections primarily remained ipsilateral across the three experimental approaches [20] and targeted the dorsolateral sector of Pf (Figure 20A-C).

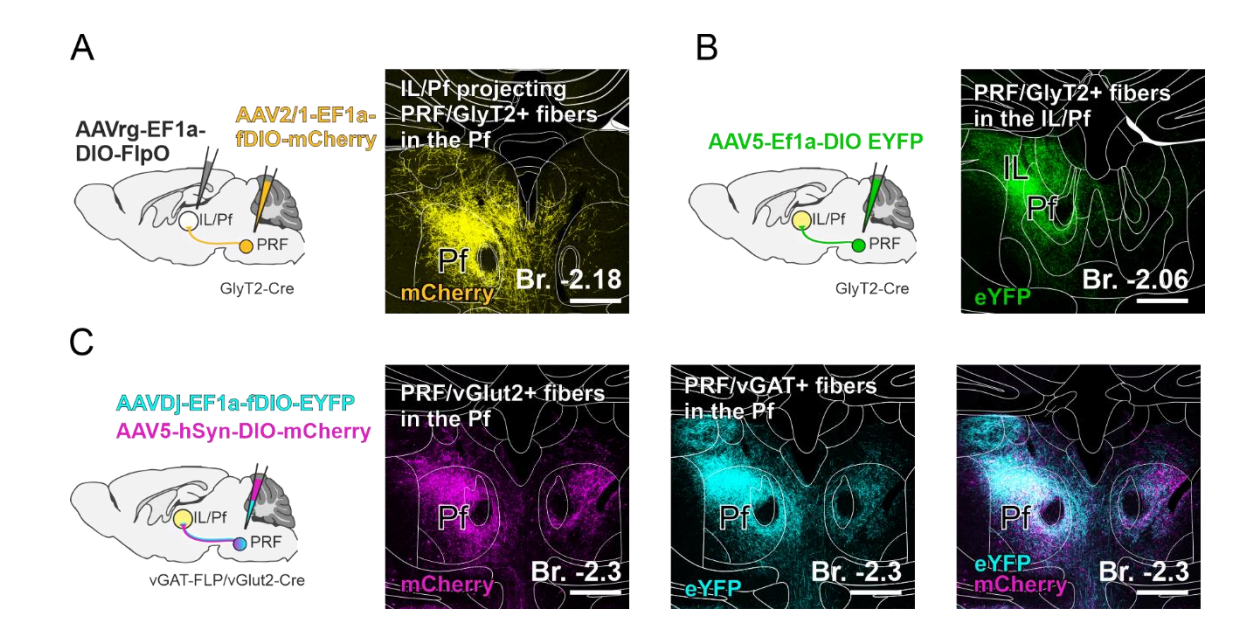


Figure 20) Thalamic innervation from different PRF sources

A) Scheme of double conditioned viral tracing for investigating the thalamus-projecting PRF/GlyT2+ cells' efferents in GlyT2-Cre mice (right) and their axons in the thalamus (left). B) Experimental design to label all PRF/GlyT2+ cells (left) and their axons in the thalamus (right). C) Scheme of mixed viral injection into PRF in vGAT-Flp/vGlut2-Cre (right) and their vGlut2+ fibers (magenta); PRF/vGAT+ fibers (cyan) and merged confocal image of the vGlut2+ and vGAT+ fibers (left) in the Pf. Scale bars: A-C) 500 µm [32]

Additionally, thalamus-projecting PRF/GlyT2+ cells innervate several other ipsilateral regions, including the basal forebrain, hypothalamic areas, and the periaqueductal grey, which are not known to be involved in turning behavior (Figure 21A-G) and are not targeted by thalamus-projecting BG cells [16]. These data indicate that thalamus-projecting PRF/GlyT2+ cells comprise a specific subpopulation characterized by a primarily ipsilateral projection pattern distinct from the BG outputs.

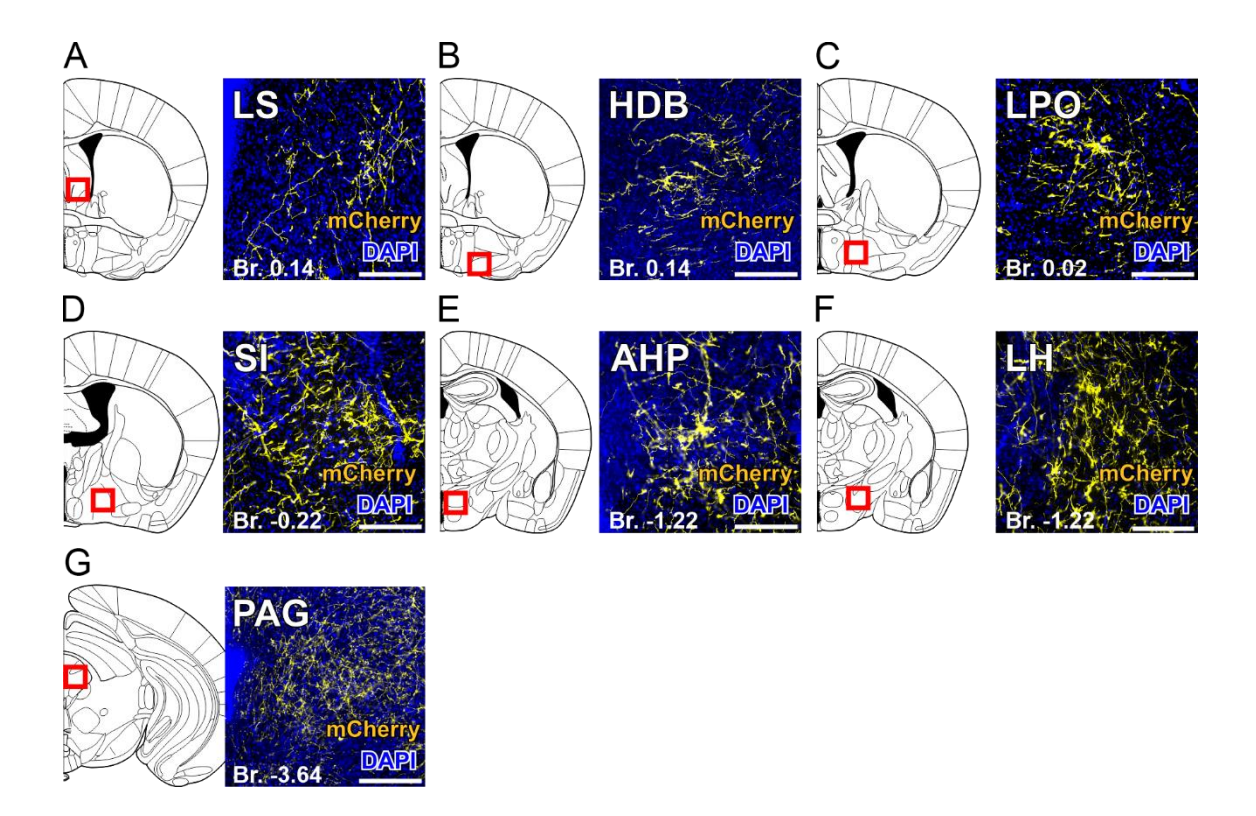


Figure 21) Efferents of thalamus-projecting PRF/GlyT2+

Representative images showing thalamus-projecting PRF/GlyT2+ axons in distinct target regions: **A)** lateral septum (LS), **B)** nucleus of the horizontal limb of the diagonal band (HDB), **C)** lateral preoptic area (LPO), **D)** substantia innominata (SI), **E)** anterior hypothalamus (AHP), **F)** lateral hypothalamus (LH), **G)** periaqueductal grey (PAG). Scale bars: A-G) 200 μ m [32]

These experiments confirm the presence of an thalamus-projecting glycinergic PRF cell population that primarily projects to the ipsilateral Gi, and the activation of these cells can have synergistic behavioral effects with the contralaterally projecting excitatory PRF neurons.

Chapter summary

- Thalamus-projecting PRF/GlyT2+ neurons preferentially innervate the ipsilateral gigantocellular nucleus (Gi), whereas the whole PRF/GlyT2+ population shows bilateral projections to the Gi.
- Excitatory vGlut2+ PRF neurons predominantly project to the contralateral Gi
- ➤ PRF/vGAT+ neurons project bilaterally but with ipsilateral dominance
- ➤ Thalamus-projecting PRF/GlyT2+ cells innervate several other brain areas wich are not connected to motor functions

4.7. ELECTROPHYSIOLOGICAL RECORDINGS OF M2 NEURONS

We showed that the cortex–PRF–thalamus forms multiple embedded loops, and this network is actively involved in motor behavior, as indicated by rotation during stimulation. Next, we aimed to investigate the optogenetic response properties of the M2/Cg L5 neurons in the Thy1-Chr2-EGFP mouse line, where each L5 neuron expresses ChR2 and EGFP [60]. However, the exact electrophysiological properties of the evoked response in L5 have not been characterized; it is unknown what the probability is of firing L5 cells at different laser intensities and stimulation frequencies (57).

We photostimulated the L5 neurons and recorded their responses using the in vivo juxtacellular recording method in anesthetized mice (Figure 22A; n=13 cells across n=5 mice). The experimental protocol involved optogenetic stimulation of L5 neurons at different frequencies (1 Hz, 10 Hz, and 20 Hz) and laser intensities ranging from 0.035 mW mW to 10 mW (Figure 22B, intensities were the following (mW): 0,035; 0,075; 0,15; 03; 0,625; 1,25; 2,5; 5; and 10). We analyzed the response probability and latency of M2/Cg L5 neurons to quantify the relationship between laser power and neuronal activation.

The response probability increased steeply with increasing laser intensity. Across individual neurons, responses followed an all-or-none pattern, with some cells showing lower activation thresholds and others requiring higher laser power (Figure 22B-C). The average population response probability curve revealed a clear dose-response relationship, with saturation approaching 100% at 10 mW. Increasing the stimulation frequency to 10 or 20 Hz yielded similar results, albeit at 20 Hz, the response probabilities of two neurons dropped at high powers; thus, the population response did not reach 100% (Figure 22B; 1 Hz: 99%, 10 Hz: 98%, and 20 Hz: 85%). This was supported by a strong positive Spearman correlation between laser power and mean response probability: $\rho = 0.996$ (p < 0.001) at 1 Hz, $\rho = 0.983$ (p < 0.001) at 10 Hz, and $\rho = 0.983$ (p < 0.001) at 20 Hz. These results confirm that increasing laser intensity leads to higher recruitment probability.

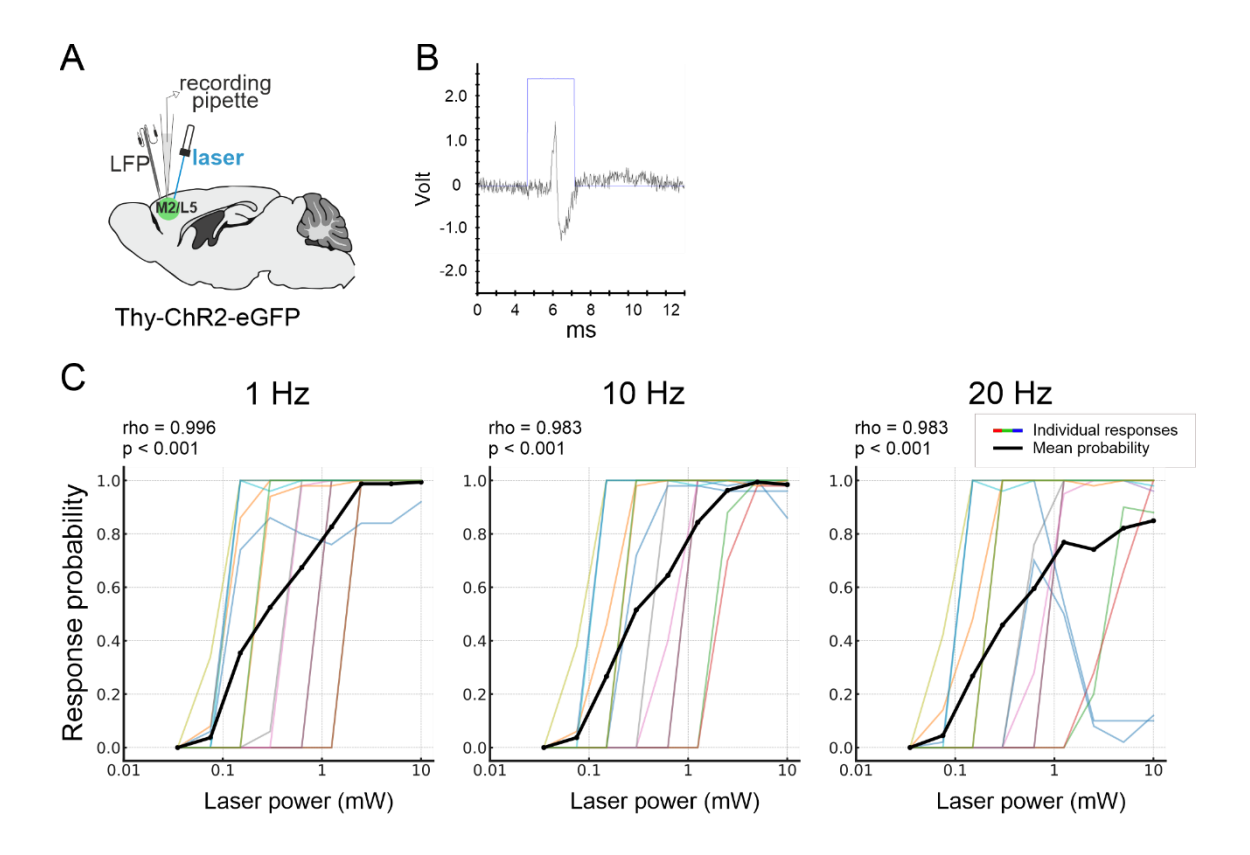


Figure 22) In vivo juxtacellular recordings reveal reliable optogenetic activation of M2/Cg L5 neurons

A) Schematic illustration of the in vivo experimental setup, indicating the position of the optical fiber and recording electrode targeting M2/Cg L5 neurons. **B)** Representative laser stimulus (blue) with the evoked action potential (AP) response **C)** Individual response probabilities of M2/Cg neurons across different laser intensities at three stimulation frequencies with Spearman's rho value: 1 Hz (left), 10 Hz (middle), and 20 Hz (right). Each colored line represents one neuron, while the black line displays the mean probability values across frequencies [60]

Next, when we analyzed the latency, we observed an inverse correlation with laser intensity, with shorter response times at higher power (Figure 23A). This trend was consistent across all stimulation frequencies (1–20 Hz), indicating that stronger stimulation not only increased the likelihood of spike generation but also accelerate the timing of responses (Spearman's rho values were -0.893 (p = 0.012) for 1 Hz, -0.929 (p = 0.002) for 10 Hz, and -0.786 (p = 0.028) for 20 Hz). The mean latencies showed a clear decline with increasing intensity at 1 Hz from 7.3 ms to 3.5 ms; at 10 Hz from 8.4 ms to 3.6 ms; and 20 Hz from 9.2 ms to 4.3 ms. At low intensities, latencies were longer, while higher intensities produced faster and more reliable responses.

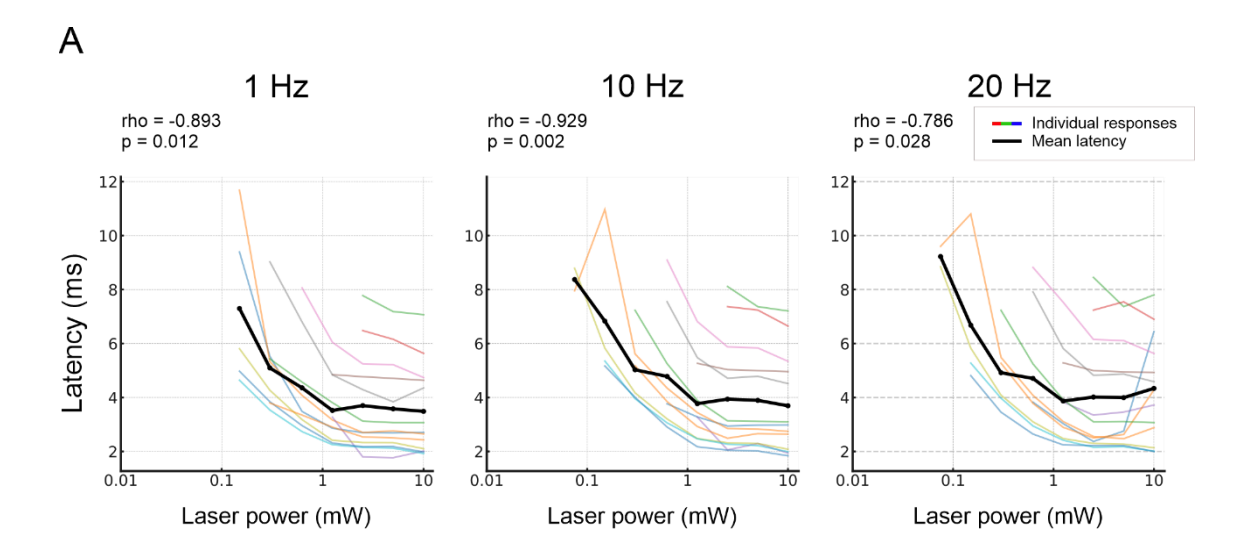


Figure 23) Response latencies of M2/Cg L5 neurons decrease with increasing laser intensity

A) Individual latency values across laser intensities at different stimulation frequencies with Spearman's rho: 1 Hz (left), 10 Hz (middle), and 20 Hz (right). Each gray line represents one neuron, while the black line displays the mean latency values across frequencies.

Next, we aimed to validate the M2–PRF connection using electrophysiological recordings. Although I did not personally conduct these experiments (and therefore do not detail them in the Methods section), they are closely related to my findings and serve to support them. For this reason, a brief discussion is warranted.

These electrophysiological recordings further underscore the functional relevance of the M2/Cg-PRF/GlyT2 circuitry. In vitro patch clamp recordings demonstrated that optogenetic activation of M2/Cg terminals evokes fast, glutamatergic synaptic responses in PRF/GlyT2+ neurons with minimal short-term depression [32]. In addition, in vivo juxtacellular recordings from anesthetized animals showed that both optogenetic and electrical stimulation of M2/Cg consistently induced spikes in PRF/GlyT2+ neurons, with high probability even at frequencies of up to 20 Hz. PRF/GlyT2+ neurons were also found to be phase-locked to cortical oscillations, firing at specific points in the up-down cycle, which indicates a tight coupling between cortical state and PRF output [32].

This result provides insights into the electrophysiological dynamics of L5 neurons and their functional implications in cortical circuitry. This suggests that this population can be effectively recruited for downstream activation of PRF neurons, but the response probability and timing depend on the laser intensity and frequency used. Furthermore,

these findings collectively confirm a robust and faithful excitatory influence of the M2/Cg cortex on PRF/GlyT2+ neurons, highlighting this pathway as a functionally relevant and dynamic component of cortico-brainstem motor circuitry.

Chapter summary

- ➤ M2/Cg L5 neurons reliably fire in response to optogenetic stimulation in an all-ornone fashion, with recruitment strength strongly correlating with laser intensity
- Response latencies decrease with increasing laser power, suggesting faster signal transduction at higher intensities.
- > Stimulation frequency has minimal impact on the probability and latency profiles, supporting consistent excitability across physiologically relevant firing rates.

5. DISCUSSION

5.1. OVERVIEW

Our research reveals a cortico-subcortical loop that includes the M2/Cg, the PRF, and the thalamus. Both anatomical and functional data align to demonstrate that this loop creates a nested feedback system, allowing precise modulation of motor output (Figure 24). Anatomically, M2/Cg layer 5 neurons project robustly to the rostral PRF (or PnO), targeting neurons that express the glycine transporter 2. These projections exhibit a clear rostrocaudal and lateromedial gradient and form monosynaptic contacts with the dendrites and spines of PRF/GlyT2+ neurons. Importantly, a substantial proportion of thalamus-projecting PRF/GlyT2+ neurons receive direct cortical input, suggesting that these cells serve as a major node for cortical control over thalamic inhibition. The application of double-conditional viral tracing and the analysis of MouseLight reconstructions further supported the presence of collaterals from individual L5 neurons to both the PRF and the IL/Pf thalamic nuclei, with some also innervating the striatum (Figure 24). These findings highlight a nested loop architecture within the cortex-PRF-thalamus axis, where individual cortical neurons interface both directly with the thalamus and indirectly via a PRF/GlyT2+ transfer.

Functionally, the eletropsychological results reveal that L5 neurons in the M2/Cg cortex exert a robust, reliable excitatory influence on PRF/GlyT2+ neurons, positioning this pathway as a dynamic component of cortico-brainstem motor circuitry. Their recruitment for downstream activation depends on laser intensity and frequency, which shape response probability and timing.

The manipulation of PRF/GlyT2+ neurons reveals complex outcomes on behavior. Photostimulation of their axons in the thalamus consistently induces contralateral turning or behavioral arrest [20]. At the same time, broader activation or inhibition of the entire PRF/GlyT2+ population yields more variable effects, including both ipsi- and contraversive rotations. The lack of consistent dose-response relationships suggests that the circuit's output is not solely dictated by stimulation intensity.

We explain the variable output of turning behavior by the results of our projectionspecific analyses in the PRF. These experiments revealed that thalamus-projecting PRF/GlyT2+ neurons selectively innervate the ipsilateral Gi (Figure 24). Inhibition of the ipsilateral Gi that mediates contralateral turning (18). This is why we think the stimulation of PRF/GlyT2+ axon in the thalamus results in contralateral turning via antidromic activation of PRF/GlyT2+ neurons that project to ipsi Gi. We also found, however, that (17) the PRF/vGAT+ cells (which include GlyT2+ cells) project bilaterally (Figure 24). This is only possible if the non-thalamus projecting PRF inhibitory cells target contralateral Gi, which mediates ipsilateral turning. This dichotomy suggests that, depending on exactly which inhibitory PRF neurons are activated in the PRF (when we stimulate PRF somata), the final motor output can be both ipsi- and contralateral turning, depending on their downstream targets.

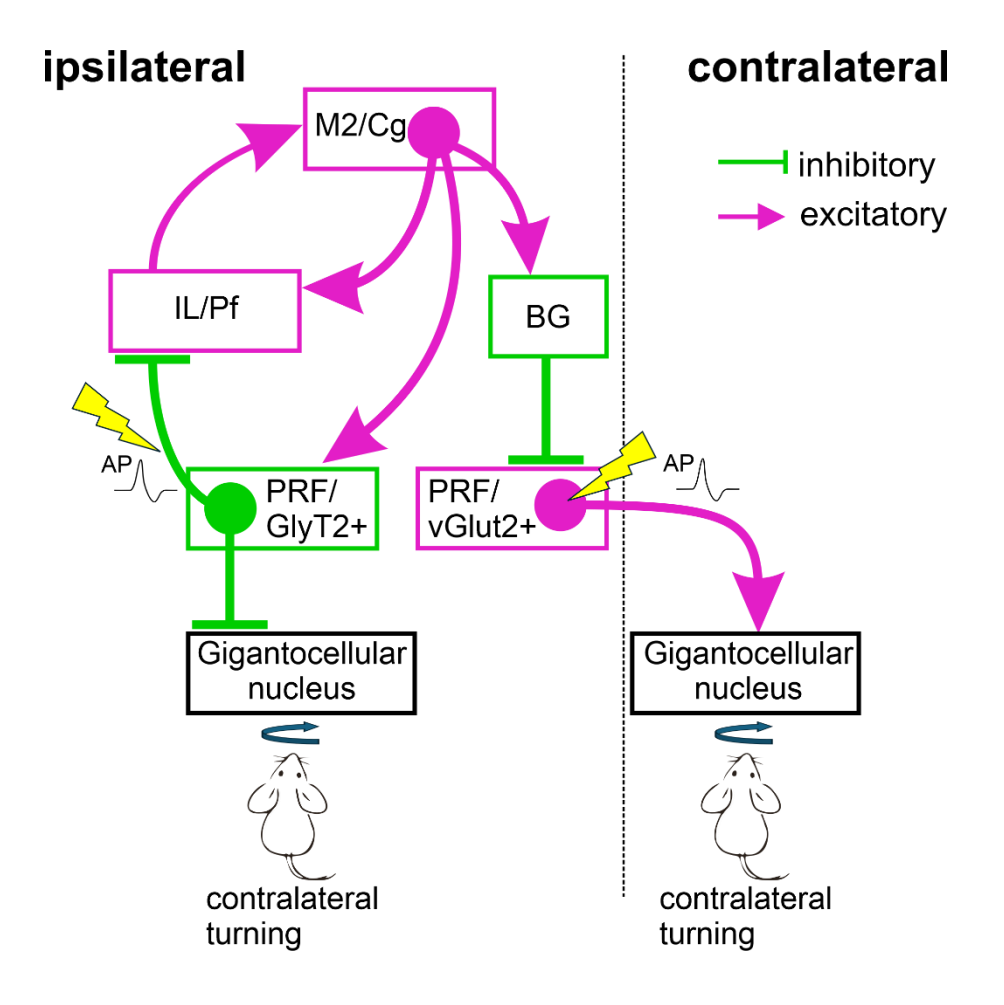


Figure 24) Cortico-brainstem thalamic circuit that controls motor activity

Left: PRF/Glyt2+ neurons receive motor cortical inputs, which also target the thalamus and the basal ganglia, forming a regulatory loop. In turn, PRF/GlyT2+ neurons inhibit the ipsilateral thalamus and medulla and drive contralateral turning. Right: PRF/vGlut2+ neurons project contralaterally to the Gi and promote contralateral turning [32]

5.2. BG-THALAMUS AND PRF-THALAMUS CIRCUITS IN MOTOR REGULATION

Within the broader functional architecture of motor circuits, now we can claim that two prominent cortico-subcortical loops control motor activity: the well-established cortico-basal ganglia—thalamocortical (C-BG-T) loop and the now proposed cortico—pontine reticular formation—thalamus (C-PRF-T) loop. Both loops demonstrate a nested loop organisation with the cortex and thalamus, including inhibitory subcortical stations and share some fundamental common organizing principles. At the same time, they also exhibit distinct features in their pathways and functional contributions.

In C-PRF-T loop M2/Cg directly targets and strongly controls the activity of GlyT2+ cells in the PRF, which, in turn, project to and powerfully inhibit the IL/Pf of the thalamus. Thus, PRF inputs overlap with the BG inputs in these nuclei. The synaptic organization of the BG-IL/Pf and PRF/GlyT2+-IL/Pf pathway is very similar. they form large multisynaptic inhibitory terminals that are able to exert strong non-depressing inhibitory action on their targets [20,32]. Crucially, M2/Cg neurons co-innervate both PRF/GlyT2+ cells, the IL/Pf, forming a nested loop organisation similar to the L5 cortico-IL/Pf cells that also target the striatum.

The C-PRF-T loop regulates motor activity parallel to C-BG-T loops. Activation of thalamus-projecting PRF/GlyT2+ cells leads to contralateral turning [32]. The PRF/GlyT2+ cells strongly inhibit IL/Pf neuronal activity in vivo; therefore, this inhibition is suggested to be crucial for fine control of thalamocortical circuits [32]. The cortical action on PRF and the BG can synergistically affect turning behavior via differential action on ipsi- vs. contralateral reticulospinal neurons [17,32]. Different circuit elements responsible for ipsi- or contralateral rotation in the PRF are intermingled.

In summary, both loops are crucial for motor control and locomotion. Both systems exhibit a nested loop structure where cortical signals return to the cortex via direct thalamo-cortical projections and an indirect loop passing through an intermediate subcortical structure (BG or PRF) before the thalamus [32]. Both receive strong excitatory input from Layer 5 pyramidal neurons in the cortex, which also project directly to the thalamus [29,32].

While the C-BG-T loop uses the BG as the primary subcortical processing unit [6,7], the C-PRF-T loop uses the pontine reticular formation, specifically GlyT2+ cells [32]. The

C-BG-T loops involve a wider range of thalamic nuclei (IL/Pf and ventromedial as well) with topographic segregation [7]. The C-PRF-T loop specifically targets the IL/Pf. Apart from the thalamus, the two loops target distinct regions or cell types in the brainstem. The BG projections reach the superior colliculus and other brainstem areas like PPN and CnF, and PRF/vGlut2+ cells [1,2,17], BG does not project to the PRF/GlyT2+ neurons[17]. The thalamus-projecting PRF/GlyT2+ cells project to the ipsilateral medulla, distinct from BG PRF/vGlut+ contralateral medullary projections, and do not receive afferents from SNr. The C-BG-T network is highly modular, composed of six parallel subnetworks that sequentially transduce specific subsets of cortical information [7] but the C-PRF-T subnetworks are undiscovered. A major difference between the two systems is that whereas the C-PRF-T pathway utilizes a single subcortical GABAergic station (the PRF), the C-BG-T loop has a complex network of direct and indirect pathways. This indicates a more complex transformation of the original cortical signal, in the case of the C-BG-T loop, before it reaches the thalamus as an inhibitory spike train.

Cortical activity can influence both PRF and BG, which can synergistically affect motor actions like turning. C-BG-T loop supports complex functions like action selection, model-based learning, and context-dependent behaviour [33,34]. The C-PRF-T loop is highlighted for its role in regulating motor activity parallel to the BG and its specific influence on turning behavior; other functions, for example, arousal or attention, need to be investigated [32]. The C-BG-T loop is extensively implicated in PD due to widespread connectivity with the entire BG network and significant cell loss in PD patients, meanwhile, the involvement of the C-PRF-T loop in PD or other movement and non-movement related diseases is unknown [35,44,56,61].

In conclusion, the cortex processes information for motor control through multiple, distinct, yet potentially synergistic, cortico-subcortical loops. The C-BG-T loop is a complex, highly organised system with multiple parallel subnetworks crucial for diverse motor, cognitive, and limbic functions, deeply intertwined with action selection and learning. The C-PRF-T loop, while also a cortico-subcortical circuit receiving similar cortical inputs, provides a parallel pathway primarily for motor control, specifically demonstrated to influence turning behaviour through its inhibitory action on the IL/Pf.

These findings highlight the sophisticated multi-loop architecture of the brain, where different pathways can collaborate to achieve complex motor behaviours. The IL/Pf stands at the intersection of these loops, integrating signals from multiple brainstem and BG sources to shape contextually appropriate motor outputs. This integrated perspective invites a reassessment of how we conceptualize motor control and may offer new insights into the pathophysiology of movement disorders, where dysfunction in one or both of these circuits could disrupt the delicate balance of inhibition and excitation required for fluid, adaptive behavior.

5.3. LIMITATIONS OF THE STUDY

This study leaves several important avenues open for further exploration. First, many cortical terminals contacted GlyT2-negative neurons in the PRF, and this raises the possibility that additional populations, such as PRF/vGlut2+ neurons, may also receive cortical input. However, the nature and functional relevance of these potential synaptic connections remain to be determined.

Second, we found that in addition to inhibitory PRF neurons, excitatory vGlut2+ PRF cells also project to the same region within the IL/Pf. This suggests a potentially complex "push–pull" regulatory mechanism between the PRF and IL/Pf. Furthermore it suggests that the C-PRF-T loop may contain also an excitatory component..

Third our tracing data revealed that while PRF/GlyT2+ neurons innervate both sides of the Gi relatively symmetrically, vGAT+ projections show a pronounced ipsilateral preference. Given that all GlyT2+ neurons are also vGAT+, this observation implies the existence of a vGAT-positive/GlyT2-negative subset within the PRF, which may contribute substantially to ipsilateral inhibition and therefore influence contralateral turning behavior [20].

Finaly, our data do not conclusively resolve whether the observed turning and orienting responses are mediated solely by ascending projections to the thalamus, descending collaterals to the Gi, or a combination of both. Previous studies have shown that inhibition of either the Pf or Gi alone can produce contralateral turning biases, which suggests that both efferent branches of PRF/GlyT2+ neurons might collaborate to orchestrate motor

orientation [17,18,20]. Definitive resolution of this question will require future investigations with pathway-specific manipulations.

6. CONCLUSION

In conclusion, based on our data, we propose the existence of a cortico-PRF-thalamus loop (C-PRF-T) that functions alongside the widely recognized cortico-basal ganglia-thalamocortical loops (C-BG-T). Both share structural and functional similarities, converge on the same thalamic nuclei, the IL/Pf, and synergistically contribute to motor control, utilizing parallel descending pathways.

When considering the broader functional architecture of motor circuits, our data suggest that the C-PRF-T loop may operate in parallel with the established C-BG-T loops. The C-BG-T modulates motor behavior through inhibitory projections from the SNr to PRF/vGlut2+ neurons, which then excite the contralateral Gi and promote contralateral turning [17]. Conversely, in the C-PRF-T loop the PRF/GlyT2+ neurons inhibits the ipsilateral Gi, which also facilitates contralateral turning. These complementary pathways highlight the importance of converging yet distinct mechanisms for motor control, with cortical layer 5 neurons acting as key regulators of both thalamic and brainstem targets.

The nested loop configuration observed here, where M2/Cg projects to both IL/Pf and PRF/GlyT2+ neurons (and the striatum as well), and these PRF neurons in turn project back to IL/Pf, adds a layer of regulatory complexity. This organization may allow the system to fine-tune thalamic excitability and adapt motor output in response to cortical dynamics. The dual outputs of PRF/GlyT2+ neurons—thalamic inhibition and descending inhibition of brainstem nuclei—position them as central integrators of cortically driven motor modulation.

Collectively, these findings support the existence of a cortico-PRF-thalamus loop that contributes to voluntary movement control by directly modulating both thalamic and brainstem structures. This loop complements traditional BG-thalamocortical circuits and provides an additional substrate for adaptive and flexible motor behavior. Our anatomical, behavioral, and physiological data converge to describe a system in which cortical neurons facilitate feedforward inhibition through PRF neurons, enhancing our understanding of distributed motor control in the mammalian brain.

7. SUMMARY

Based on the thesis, this research examines a cortex-PRF-thalamus circuit that plays a role in motor function control. Anatomical tracing revealed that M2/cingulate (Cg) cortical layer 5 (L5) neurons densely innervate PRF neurons expressing GlyT2+, forming a dense axon arbor in the rostral PRF with a rostrocaudal increase in fibre density. Ultrastructural analysis confirmed monosynaptic contacts between M2/Cg terminals and PRF/GlyT2+ neurons, primarily targeting dendrites and spines. Furthermore, M2/Cg terminals form close appositions with thalamus-projecting PRF/GlyT2+ dendrites. Single L5 neurons can co-innervate both the PRF and the intralaminar/parafascicular (IL/Pf) thalamus, with many also projecting to the striatum. Two experimental designs further demonstrated that thalamus-projecting cortical neurons also innervate PRF/GlyT2+ cells, establishing a nested loop organisation. Functional investigations showed that photostimulation of PRF/GlyT2+ fibres in the IL/Pf thalamus induces contralateral rotational movements. Somatic photoactivation of PRF/GlyT2+ neurons can result in both contraversive and ipsiversive rotational movements, as well as movement initiation. Importantly, thalamus-projecting PRF/GlyT2+ neurons preferentially innervate the ipsilateral gigantocellular nucleus (Gi), while the entire PRF/GlyT2+ population projects bilaterally to the Gi. Excitatory vGlut2+ PRF neurons mainly project contralaterally to the Gi, and PRF/vGAT+ neurons project bilaterally with ipsilateral dominance. Electrophysiological recordings confirmed that M2/Cg L5 neurons reliably fire in response to optogenetic stimulation.

In conclusion, the thesis supports the existence of a cortex-PRF-thalamus loop that operates in parallel to BG loops for motor control. Cortical L5 neurons influence thalamic activity via inhibitory PRF/GlyT2+ neurons, which also project to brainstem motor centres like the Gi, suggesting a complex interplay for precise movement coordination and the generation of turning movements.

8. References

- Arber S, Costa RM. Networking brainstem and basal ganglia circuits for movement. Nature Reviews Neuroscience 2022 23:6 [Internet]. 2022 Apr 14 [cited 2022 May 23];23(6):342–60. Available from: https://www.nature.com/articles/s41583-022-00581-w
- Leiras R, Cregg JM, Kiehn O. Brainstem Circuits for Locomotion. Annu Rev Neurosci [Internet]. 2022 Jul 1 [cited 2023 May 20];45:63–85. Available from: https://pubmed.ncbi.nlm.nih.gov/34985919/
- 3. Smith Y, Raju D V., Pare JF, Sidibe M. The thalamostriatal system: A highly specific network of the basal ganglia circuitry. Vol. 27, Trends in Neurosciences. Trends Neurosci; 2004. p. 520–7.
- 4. Cui G, Jun SB, Jin X, Pham MD, Vogel SS, Lovinger DM, Costa RM. Concurrent activation of striatal direct and indirect pathways during action initiation. Nature. 2013 Feb 14;494(7436):238–42.
- Díaz-Hernández E, Contreras-López R, Sánchez-Fuentes A, Rodríguez-Sibrían L, Ramírez-Jarquín JO, Tecuapetla F. The Thalamostriatal Projections Contribute to the Initiation and Execution of a Sequence of Movements. 2018 [cited 2022 Feb 16]; Available from: https://doi.org/10.1016/j.neuron.2018.09.052
- 6. Hintiryan H, Foster NN, Bowman I, Bay M, Song MY, Gou L, Yamashita S, Bienkowski MS, Zingg B, Zhu M, Yang XW, Shih JC, Toga AW, Dong HW. The mouse cortico-striatal projectome. Nature Neuroscience 2016 19:8 [Internet]. 2016 Aug 1 [cited 2023 Jul 6];19(8):1100–14. Available from: https://www.nature.com/articles/nn.4332
- 7. Foster NN, Barry J, Korobkova L, Garcia L, Gao L, Becerra M, Sherafat Y, Peng B, Li X, Choi JH, Gou L, Zingg B, Azam S, Lo D, Khanjani N, Zhang B, Stanis J, Bowman I, Cotter K, Cao C, Yamashita S, Tugangui A, Li A, Jiang T, Jia X, Feng Z, Aquino S, Mun HS, Zhu M, Santarelli A, Benavidez NL, Song M, Dan G, Fayzullina M, Ustrell S, Boesen T, Johnson DL, Xu H, Bienkowski MS, Yang XW, Gong H, Levine MS, Wickersham I, Luo Q, Hahn JD, Lim BK, Zhang LI,

- Cepeda C, Hintiryan H, Dong HW. The mouse cortico—basal ganglia—thalamic network. Nature [Internet]. 2021 Oct 7 [cited 2023 Jul 14];598(7879):188. Available from: /pmc/articles/PMC8494639/
- 8. Alexander GE, DeLong MR, Strick PL. Parallel Organization of Functionally Segregated Circuits Linking Basal Ganglia Cortex. and https://doi.org/101146/annurev.ne09030186002041 [Internet]. 2003 Nov 28 [cited 2023 Jul 9:357-81. Available 6];VOL. from: https://www.annualreviews.org/doi/abs/10.1146/annurev.ne.09.030186.002041
- Acsády L. Heterogeneity of Thalamic Input Landscapes. The Cerebral Cortex and Thalamus [Internet]. 2023 Nov 1 [cited 2024 Aug 23];32–44. Available from: https://academic.oup.com/book/55212/chapter/427108580
- 10. Jaramillo J, Guo Z V. Thalamocortical Contributions to Neural Dynamics and Behavior. The Cerebral Cortex and Thalamus [Internet]. 2023 Nov 1 [cited 2024 Aug 23];367–80. Available from: https://academic.oup.com/book/55212/chapter/427110609
- McNaughton N, Vann SD. Construction of complex memories via parallel distributed cortical-subcortical iterative integration. Trends Neurosci [Internet].
 Jul 7 [cited 2024 Aug 21];45(7):550. Available from: /pmc/articles/PMC7612902/
- 12. Berendse HW, Groenewegen HJ. Organization of the thalamostriatal projections in the rat, with special emphasis on the ventral striatum. J Comp Neurol [Internet]. 1990 [cited 2023 Jul 14];299(2):187–228. Available from: https://pubmed.ncbi.nlm.nih.gov/2172326/
- 13. Pare D, Smith Y. Thalamic Collaterals of Corticostriatal Axons: Their Termination Field and Synaptic Targets in Cats. J Comp Neurol [Internet]. 1996 [cited 2023 Aug 4];372–551. Available from: https://onlinelibrary.wiley.com/doi/10.1002/
- 14. Levesque M, Gagnon S, Parent A, Deschenes. Axonal arborizations of corticostriatal and corticothalamic fibers arising from the second somatosensory area in the rat. Cereb Cortex. 1996;6(6):759-70.

- Economo MN, Viswanathan S, Tasic B, Bas E, Winnubst J, Menon V, Graybuck LT, Nguyen TN, Smith KA, Yao Z, Wang L, Gerfen CR, Chandrashekar J, Zeng H, Looger LL, Svoboda K. Distinct descending motor cortex pathways and their roles in movement. Nature [Internet]. 2018;563(7729):79–84. Available from: http://dx.doi.org/10.1038/s41586-018-0642-9
- 16. McElvain LE, Chen Y, Moore JD, Brigidi GS, Bloodgood BL, Lim BK, Costa RM, Kleinfeld D. Specific populations of basal ganglia output neurons target distinct brain stem areas while collateralizing throughout the diencephalon. Neuron [Internet]. 2021 May 19 [cited 2023 Jan 5];109(10):1721-1738.e4. Available from: https://pubmed.ncbi.nlm.nih.gov/33823137/
- 17. Cregg JM, Sidhu SK, Leiras R, Kiehn O. Basal ganglia—spinal cord pathway that commands locomotor gait asymmetries in mice. Nature Neuroscience 2024 27:4 [Internet]. 2024 Feb 12 [cited 2024 Apr 9];27(4):716–27. Available from: https://www.nature.com/articles/s41593-024-01569-8
- Goñi-Erro H, Selvan R, Caggiano V, Leiras R, Kiehn O. Pedunculopontine Chx10+ neurons control global motor arrest in mice. Nature Neuroscience 2023 [Internet]. 2023 Jul 27 [cited 2023 Aug 14];1–13. Available from: https://www.nature.com/articles/s41593-023-01396-3
- 19. Cregg JM, Leiras R, Montalant A, Wanken P, Wickersham IR, Kiehn O. Brainstem neurons that command mammalian locomotor asymmetries. Nat Neurosci [Internet]. 2020 Jun 1 [cited 2023 Jan 5];23(6):730–40. Available from: https://pubmed.ncbi.nlm.nih.gov/32393896/
- 20. Giber K, Diana MA, M Plattner V, Dugué GP, Bokor H, Rousseau C V, Maglóczky Z, Havas L, Hangya B, Wildner H, Zeilhofer HU, Dieudonné S, Acsády L. A subcortical inhibitory signal for behavioral arrest in the thalamus. Nat Neurosci [Internet]. 2015 Feb 23 [cited 2015 Feb 23];18(4):562–8. Available from: http://www.ncbi.nlm.nih.gov/pubmed/25706472
- 21. Zeilhofer HU, Studler B, Arabadzisz D, Schweizer C, Ahmadi S, Layh B, Bösl MR, Fritschy JM. Glycinergic neurons expressing enhanced green fluorescent protein in bacterial artificial chromosome transgenic mice. J Comp Neurol

- [Internet]. 2005 Feb 7 [cited 2023 Aug 4];482(2):123–41. Available from: https://pubmed.ncbi.nlm.nih.gov/15611994/
- 22. Halassa MM, Acsády L. Thalamic Inhibition: Diverse Sources, Diverse Scales. Trends Neurosci. 2016;39(10).
- 23. Fallon IP, Hughes RN, Severino FPU, Kim N, Lawry CM, Watson GDR, Roshchina M, Yin HH. The role of the parafascicular thalamic nucleus in action initiation and steering. Current Biology [Internet]. 2023 Jul 24 [cited 2025 May 29];33(14):2941-2951.e4. Available from: https://www.cell.com/action/showFullText?pii=S0960982223007765
- 24. Watson GDR, Hughes RN, Petter EA, Fallon IP, Kim N, Severino FPU, Yin HH. Thalamic projections to the subthalamic nucleus contribute to movement initiation and rescue of parkinsonian symptoms. Sci Adv [Internet]. 2021 Feb 5 [cited 2023 Jan 5];7(6). Available from: https://pubmed.ncbi.nlm.nih.gov/33547085/
- 25. Matsumoto N, Minamimoto T, Graybiel AM, Kimura M. Neurons in the thalamic CM-Pf complex supply striatal neurons with information about behaviorally significant sensory events. J Neurophysiol. 2001;85(2):960–76.
- 26. Minamimoto T, Kimura M. Participation of the thalamic CM-Pf complex in attentional orienting. J Neurophysiol [Internet]. 2002 [cited 2024 Aug 26];87(6):3090–101. Available from: https://pubmed.ncbi.nlm.nih.gov/12037210/
- 27. Vertes RP, Linley SB, Rojas AKP. Structural and functional organization of the midline and intralaminar nuclei of the thalamus. Front Behav Neurosci. 2022 Aug 23;16:964644.
- 28. Sidibé M, Paré JF, Smith Y. Nigral and pallidal inputs to functionally segregated thalamostriatal neurons in the centromedian/parafascicular intralaminar nuclear complex in monkey. J Comp Neurol [Internet]. 2002 Jun 3 [cited 2023 Jan 5];447(3):286–99. Available from: https://pubmed.ncbi.nlm.nih.gov/11984822/
- 29. Gonzalo-Martín E, Alonso-Martínez C, Sepúlveda LP, Clasca F. Micropopulation mapping of the mouse parafascicular nucleus connections reveals diverse input–output motifs. Front Neuroanat. 2023 Jan 8;17:1305500.

- 30. Ichinohe N, Mori F, Shoumura K. A di-synaptic projection from the lateral cerebellar nucleus to the laterodorsal part of the striatum via the central lateral nucleus of the thalamus in the rat. Brain Res [Internet]. 2000 Oct [cited 2016 Jan 27];880(1–2):191–7. Available from: http://www.sciencedirect.com/science/article/pii/S000689930002744X
- 31. Chen CH, Fremont R, Arteaga-Bracho EE, Khodakhah K. Short latency cerebellar modulation of the basal ganglia. Nat Neurosci [Internet]. 2014 Dec [cited 2016 Jan 27];17(12):1767–75. Available from: http://dx.doi.org/10.1038/nn.3868
- 32. Bősz E, Plattner VM, Biró L, Kóta K, Diana MA, Acsády L. A cortico-subcortical loop for motor control via the pontine reticular formation. Cell Rep [Internet]. 2025 Feb [cited 2025 Jun 3];44(2):115230. Available from: https://pubmed.ncbi.nlm.nih.gov/39847485/
- 33. Mair RG, Francoeur MJ, Krell EM, Gibson BM. Where Actions Meet Outcomes: Medial Prefrontal Cortex, Central Thalamus, and the Basal Ganglia. Front Behav Neurosci [Internet]. 2022 Jul 5 [cited 2023 Feb 16];16. Available from: https://pubmed.ncbi.nlm.nih.gov/35864847/
- 34. Cruz KG, Leow YN, Le NM, Adam E, Huda R, Sur M. Cortical-subcortical interactions in goal-directed behavior. Physiol Rev [Internet]. 2023 Jan 1 [cited 2023 Feb 16];103(1):347–89. Available from: https://pubmed.ncbi.nlm.nih.gov/35771984/
- 35. Li M, Zhang X, He Q, Chen D, Chen F, Wang X, Sun S, Sun Y, Li Y, Zhu Z, Fang H, Shi X, Yao X, Sun H, Wang M. Functional Interactions Between the Parafascicular Thalamic Nucleus and Motor Cortex Are Altered in Hemiparkinsonian Rat. Front Aging Neurosci [Internet]. 2022 May 23 [cited 2025 May 29];14:800159. Available from: www.frontiersin.org
- 36. Konnova EA, Swanberg M. Animal Models of Parkinson's Disease. Parkinson's Disease: Pathogenesis and Clinical Aspects [Internet]. 2018 Dec 21 [cited 2022 Aug 11];83–106. Available from: https://www.ncbi.nlm.nih.gov/books/NBK536725/

- 37. McGregor MM, Nelson AB. Circuit Mechanisms of Parkinson's Disease. Neuron [Internet]. 2019 Mar 20 [cited 2024 Apr 22];101(6):1042–56. Available from: http://www.cell.com/article/S0896627319302119/fulltext
- 38. Kiehn O. Decoding the organization of spinal circuits that control locomotion. Nat Rev Neurosci [Internet]. 2016 Apr 1 [cited 2023 Jul 4];17(4):224. Available from: /pmc/articles/PMC4844028/
- 39. Brown RE, Basheer R, McKenna JT, Strecker RE, McCarley RW. Control of sleep and wakefulness. Physiol Rev. 2012 Jul;92(3):1087–187.
- 40. Steriade M, Contreras D, Amzica F. The thalamocortical dialogue during wake sleep and paroxysmal oscillations. In: Steriade M, Jones EG, McCormick DA, editors. Thalamus. Elsevier; 1997.
- 41. Moruzzi G, Magoun HW. Brain stem reticular formation and activation of the EEG. Electroencephalogr Clin Neurophysiol. 1949 Jan 1;1(1–4):455–73.
- 42. Schepers IM, Beck AK, Bräuer S, Schwabe K, Abdallat M, Sandmann P, Dengler R, Rieger JW, Krauss JK. Human centromedian-parafascicular complex signals sensory cues for goal-oriented behavior selection. Neuroimage. 2017 May 15;152:390–9.
- 43. Hanini-Daoud M, Jaouen F, Salin P, Kerkerian-Le Goff L, Maurice N. Processing of information from the parafascicular nucleus of the thalamus through the basal ganglia. J Neurosci Res [Internet]. 2022 Jun 1 [cited 2023 Jan 5];100(6):1370–85. Available from: https://pubmed.ncbi.nlm.nih.gov/35355316/
- 44. Arnts H, Coolen SE, Fernandes FW, Schuurman R, Krauss JK, Groenewegen HJ, Van Den Munckhof P. The intralaminar thalamus: a review of its role as a target in functional neurosurgery. Brain Commun [Internet]. 2023 [cited 2025 May 29];5(3). Available from: https://pubmed.ncbi.nlm.nih.gov/37292456/
- 45. Sadikot AF, Rymar V V. The primate centromedian–parafascicular complex: Anatomical organization with a note on neuromodulation. Brain Res Bull. 2009 Feb 16;78(2–3):122–30.

- 46. Hunter J, Jasper HH. Effects of thalamic stimulation in unanaesthetised animals; the arrest reaction and petit mal-like seizures, activation patterns and generalized convulsions. Electroencephalogr Clin Neurophysiol. 1949 Aug;1(3):305–24.
- 47. Schiff ND, Giacino JT, Kalmar K, Victor JD, Baker K, Gerber M, Fritz B, Eisenberg B, Biondi T, O'Connor J, Kobylarz EJ, Farris S, Machado a, McCagg C, Plum F, Fins JJ, Rezai a R. Behavioural improvements with thalamic stimulation after severe traumatic brain injury. Nature. 2007;448(7153):600–3.
- 48. Kinney HC, Korein J, Panigrahy A, Dikkes P, Goode R. Neuropathological Findings in the Brain of Karen Ann Quinlan The Role of the Thalamus in the Persistent Vegetative State. N Engl J Med. 1994;330(21):1469–75.
- 49. Giber K, Diana MA, Plattner VM, Dugué GP, Bokor H, Rousseau C V, Maglóczky Z, Havas L, Hangya B, Wildner H, Zeilhofer HU, Dieudonné S, Acsády L. A subcortical inhibitory signal for behavioral arrest in the thalamus. Nat Neurosci [Internet]. 2015 Apr [cited 2016 Jan 27];18(4):562–8. Available from: http://dx.doi.org/10.1038/nn.3951
- 50. Inagaki HK, Chen S, Ridder MC, Sah P, Li N, Yang Z, Hasanbegovic H, Gao Z, Gerfen CR, Svoboda K. A midbrain-thalamus-cortex circuit reorganizes cortical dynamics to initiate movement. Cell [Internet]. 2022 Mar 17 [cited 2023 Jan 5];185(6):1065-1081.e23. Available from: https://pubmed.ncbi.nlm.nih.gov/35245431/
- 51. Fang Z, Dang Y, Ping A, Wang C, Zhao Q, Zhao H, Li X, Zhang M. Human highorder thalamic nuclei gate conscious perception through the thalamofrontal loop. Science (1979) [Internet]. 2025 Apr 4 [cited 2025 May 15];388(6742). Available from: https://www.science.org/doi/10.1126/science.adr3675
- 52. Stayte S, Dhungana A, Vissel B, Bradfield LA. Parafascicular Thalamic and Orbitofrontal Cortical Inputs to Striatum Represent States for Goal-Directed Action Selection. Front Behav Neurosci [Internet]. 2021 Mar 19 [cited 2025 May 29];15:655029. Available from: www.frontiersin.org

- 53. Henderson JM, Schleimer SB, Allbutt H, Dabholkar V, Abela D, Jovic J, Quinlivan M. Behavioural effects of parafascicular thalamic lesions in an animal model of parkinsonism. Behavioural Brain Research. 2005 Jul 30;162(2):222–32.
- 54. Smith Y, Raju D, Nanda B, Pare JF, Galvan A, Wichmann T. The thalamostriatal systems: anatomical and functional organization in normal and parkinsonian states. Brain Res Bull [Internet]. 2009 Feb 16 [cited 2023 Jan 5];78(2–3):60–8. Available from: https://pubmed.ncbi.nlm.nih.gov/18805468/
- 55. Parr-Brownlie LC, Poloskey SL, Bergstrom DA, Walters JR. Parafascicular thalamic nucleus activity in a rat model of Parkinson's disease. Exp Neurol. 2009 Jun 1;217(2):269–81.
- 56. Xiao B, Tan EK. Thalamic pathways mediating motor and non-motor symptoms in a Parkinson's disease model. Trends Neurosci [Internet]. 2023 Jan 1 [cited 2025 Jun 3];46(1):1–2. Available from: https://pubmed.ncbi.nlm.nih.gov/36207171/
- 57. Schindelin J, Arganda-Carreras I, Frise E, Kaynig V, Longair M, Pietzsch T, Preibisch S, Rueden C, Saalfeld S, Schmid B, Tinevez JY, White DJ, Hartenstein V, Eliceiri K, Tomancak P, Cardona A. Fiji: an open-source platform for biological-image analysis. Nature Methods 2012 9:7 [Internet]. 2012 Jun 28 [cited 2023 Apr 5];9(7):676–82. Available from: https://www.nature.com/articles/nmeth.2019
- 58. Harris JA, Mihalas S, Hirokawa KE, Whitesell JD, Choi H, Bernard A, Bohn P, Caldejon S, Casal L, Cho A, Feiner A, Feng D, Gaudreault N, Gerfen CR, Graddis N, Groblewski PA, Henry AM, Ho A, Howard R, Knox JE, Kuan L, Kuang X, Lecoq J, Lesnar P, Li Y, Luviano J, McConoughey S, Mortrud MT, Naeemi M, Ng L, Oh SW, Ouellette B, Shen E, Sorensen SA, Wakeman W, Wang Q, Wang Y, Williford A, Phillips JW, Jones AR, Koch C, Zeng H. Hierarchical organization of cortical and thalamic connectivity. Nature [Internet]. 2019 Nov 7 [cited 2024 Sep 11];575(7781):195–202. Available from: https://pubmed.ncbi.nlm.nih.gov/31666704/
- Economo MN, Clack NG, Lavis LD, Gerfen CR, Svoboda K, Myers EW, Chandrashekar J. A platform for brain-wide imaging and reconstruction of individual neurons. Elife. 2016 Jan 20;5(JANUARY2016).

- 60. Hádinger N, Bősz E, Tóth B, Vantomme G, Lüthi A, Acsády L. Region-selective control of the thalamic reticular nucleus via cortical layer 5 pyramidal cells. Nature Neuroscience 2022 [Internet]. 2022 Dec 22 [cited 2023 Jan 5];1–15. Available from: https://www.nature.com/articles/s41593-022-01217-z
- 61. Xiao B, Tan EK. Thalamic pathways mediating motor and non-motor symptoms in a Parkinson's disease model. Trends Neurosci. 2023 Jan 1;46(1):1–2.

9. BIBLIOGRAPHY OF PUBLICATIONS

Publications related to the thesis:

Bősz Emília, Plattner Viktor M.*, Biró László*, Kóta Kata, Diana Marco A., Acsády László A cortico-subcortical loop for motor control via the pontine reticular formation CELL REPORTS 44: 2 Paper: 115230, 25 p. (2025)

Közlemény: 35713020 | Folyóiratcikk (Szakcikk) | Tudományos

Scopus - Biochemistry, Genetics and Molecular Biology (miscellaneous) SJR indikátor:

D1

IF2024: 6,9 IF2023: 7,5

Hádinger Nóra, **Bősz Emília**, Tóth Boglárka, Vantomme Gil, Lüthi Anita, Acsády László Region-selective control of the thalamic reticular nucleus via cortical layer 5 pyramidal cells NATURE NEUROSCIENCE 26: 1 pp. 116-130., 15 p. (2023) Közlemény: 33540834 | Folyóiratcikk (Szakcikk) | Tudományos Scopus - Neuroscience (miscellaneous) SJR indikátor: D1

IF2023: 21,3

 Σ IF: 28.8

Első osztott szerzős cikk, a kézirat beadásakor érvényben lévő a 2023-as if-vel számolva

^{*}osztott első szerző

10. ACKNOWLEDGEMENTS

I would like to thank László Acsády for his guidance as my supervisor and for accompanying me on my scientific journey ever since my undergraduate TDK project, all the way to completing my PhD. I'm especially grateful for the many conference opportunities he provided — I learned an incredible amount from them.

My sincere thanks go to Viktor Plattner for his mentorship during the early years of my scientific career. The knowledge and way of thinking he passed on to me laid the foundations for everything I've built since, and I'm truly grateful for that.

I would also like to thank László Biró and Nóra Hádinger — without them, my PhD project could not have come to life. Laci was an immense help during the revision process, both professionally and emotionally, and I am deeply thankful. Nóra deserves special thanks not only for introducing me to juxtacellular recordings, but also to art and galleries from all around the world. Our shared experiences and conversations turned us into true friends.

Thanks to Csaba Dávid for always cheering me up exactly when I needed it, and to Gergely Komlósi for his care and for introducing me to one of my favorite writers and thinkers, Irvin Yalom. Thank you also to Zsolt and András for the endless laughs, memories, and support.

I'm also grateful to Krisztina Faddi for her excellent technical and mental support, and for the deep conversations we had in the wet lab. A heartfelt thanks to every single member of the lab for the past 10 years.

I would also like to thank my partner, Csaba Szabó, for his endless patience, love, and encouragement, and for believing in me even when I doubted myself. In the chaos of academia, you often gave me the rhythm and the framework I needed to keep going, and for that, I will be forever grateful.

I'm also deeply thankful to my close friends — Leila, Timi, Eszter, and Czetli — who patiently accepted that I was always too busy, and who respected that this goal was my priority, showing great flexibility because of it.

Last but not least, I thank my family for all their support and for being proud of me your support was always there, steady and quiet — like a safety net I could count on. And my mother and grandmother, who never once doubted that I could find my place as a first-generation academic in the world of science, and make it to the doctoral degree. Special thanks to my mother, who often reminded me to rest, and whose hugs always recharged me. And to my grandmother, who made me fall in love with biology through her garden and the books she gave and read to me as a child. Maybe without you, Mama, I never would have become a biologist.